LOTOS-EUROS Reference Guide

v2.3.000

LOTOS-EUROS v2.3.000 Reference Guide

Date   December 2023

Author(s)   A.M.M. Manders-Groot and LOTOS-EUROS team

No. of pages   82 (incl. appendices)

Contents

1   Introduction

1.1   Air pollution modelling

In the field of large-scale air pollution, topics of investigation are atmospheric processes and the large-scale dispersion of pollutants. In addition, the interaction between climate change and air quality is gathering interest. An example of this is the role of particulate matter in climate change. Research involves using models, measurements, satellite data and data assimilation.

A key element in this research is the LOTOS-EUROS model, with which the formation and dispersion of ozone, particulate matter, nitrogen dioxide, heavy metals and persistent organic pollutants across Europe can be calculated. The standard model resolution is approximately 25 x 25 km^2 and the model offers the scope to zoom in on specific urban and industrial areas. The model makes the connection between emissions and the occurrence of concentrations and deposition.

LOTOS-EUROS is being applied and further developed by TNO with contributions from several partners. The model is being used for scientific applications and in a policy support role.

1.2   History

The development and application of chemistry transport models has a long tradition in and outside Europe. RIVM and TNO have independently developed models to calculate the dispersion and chemical transformation of air pollutants in the lower troposphere over Europe.

1.2.1   *LOTOS model*

The LOTOS (LOng Term Ozone Simulation) model originates from the US UAM (Urban Airshed Model). In the early 1970's, it were Steven Reynolds and colleagues in the group of John Seinfeld at Caltech and later at Systems Applications International (SAI), who made the pioneering attempts at photochemical air quality modelling. These efforts resulted in the UAM model, a local air quality model which was firstly designed to investigate ozone formation over Los Angelos (US). Back then, the UAM model was focused on ozone in episodic situations in urbanized areas. The present day UAM air quality modelling system is one of the most widely used photochemical air quality models in the world.

In cooperation with SAI and TNO, the UAM was modified for application over the Netherlands and its surroundings (Builtjes et al. 1980; Builtjes and Reynolds 1982). Around 1980, TNO, together with SAI, started cooperation with the FU Berlin (Free University of Berlin, meteorology department) to apply UAM for parts of Germany. UAM was extended to cover larger areas and was subsequently called RTM (Regional Transport Model). RTM was the direct predecessor of LOTOS. RTM, originally designed for the description of air quality in episodic situations, was further developed for application to longer time scales. This was done with preservation of the original UAM/RTM model features such as the representation of the mixing height - therewith making the now called LOTOS model unique in its existence. The LOTOS model, being first only focussed on ozone (Builtjes 1992), was extended around 1995 to incorporate also aerosols.

1.2.2   EUROS model

The Eulerian air quality model EUROS (EURopean Operational Smog model) was originally developed at RIVM for the modelling of winter smog (SO2) episodes in Europe (Egmond and Kesseboom 1981). Later on, the model was used for simulating various air polluting compounds, such as SOx, NOx, O3, Volatile Organic Compounds (VOCs) and Persistant Organic Pollutants (POPs) in the lower troposphere over Europe. Earlier versions of the EUROS model are described in (Jacobs and Van Pul 1996); (Loon 1994; Loon 1995), Leeuw and van Rheineck Leyssius (1990), van Rheineck Leyssius et al. (1990), (Hammingh et al. 2001; Matthijsen et al. 2001; Matthijsen et al. 2002).

1.2.3   Unification

LOTOS and EUROS were originally developed and used as photo-oxidant models (Builtjes 1992; Hass et al. 1997; Hammingh et al. 2001; Roemer et al. 2003). During the last years attention was given to simulate the inorganic secondary aerosols SO_4, NH_4 and NO_3 (Schaap et al. 2004; Erisman and Schaap 2004; Matthijsen et al. 2002) and carbonaceous aerosols (Schaap 2004). The EUROS model also contains the possibility to perform simulations for persistent organic compounds (Jacobs and Van Pul 1996). Since the two models had a similar structure and comparable application areas, based on strategic and practical reasoning, RIVM/MNP and TNO agreed to collaborate on the development of a single chemistry transport model: LOTOS-EUROS. During 2004 the two models were unified which resulted in a LOTOS-EUROS version 1.0 Schaap et al. (2005).

1.2.4   Documentation

With the development of model version 1.8 during 2011, it was decided to provide 3 documents to describe the model:

- *Reference Guide*
  The general scientific description of the model processes, including refer-ences to relevant articles and reports. A new Reference Guide is released if the previous one is outdated.

- *Validation Report*
  A validation report accompanies each new model release, and compares standard simulations with the previous and the new version with observations.

- *User Guide*
  The User Guide describes how to install and run the model, where to find the input data, and how to visualize the results. This document is part of the source code tree and updated regularly.

This report is the Reference Guide for LOTOS-EUROS v2.2, released July 1st, 2019.

1.2.5   Website

More information about LOTOS-EUROS and its applications can be found through:

   airqualitymodeling.tno.nl/lotos-euros

The website contains information on the model, online documentation, research projects in which the model is used, and contact information.

2   Model formulation and domain

2.1   The continuity equation

The main prognostic equation in the LOTOS-EUROS model is the continuity equation that describes the change in time of the concentration of a component as a result of the following processes:

- Transport

- Chemistry

- Dry and wet deposition

- Emissions.

The equation is given by:

$$
\frac{\partial C}{\partial t} + U\frac{\partial C}{\partial x} + V\frac{\partial C}{\partial y} + W\frac{\partial C}{\partial z} = \frac{\partial}{\partial x}\left(K_h\frac{\partial C}{\partial x}\right) + \frac{\partial}{\partial y}\left(K_h\frac{\partial C}{\partial y}\right) + \frac{\partial}{\partial z}\left(K_z\frac{\partial C}{\partial z}\right)
$$
$$
+ E + R + Q - D - W \tag{2.1}
$$

with C the concentration of a pollutant, U, V and W being the large scale wind components in respectively west-east direction, in south-north direction and in vertical direction. K_h and K_z are the horizontal and vertical turbulent diffusion coefficients. E represents the entrainment or detrainment due to variations in layer height. R gives the amount of material produced or destroyed as a result of chemistry. Q is the contribution by emissions, and D and W are loss terms due to processes of dry and wet deposition respectively.

In the model, the equation is solved by means of operator splitting. This means that concentration changes are calculated for separate processes:

1. chemistry

2. diffusion and entrainment

3. sedimentation

4. dry deposition

5. wet deposition

6. advection

7. emission.

For more details on the time stepping involved, one is referred to section 2.6.

In the following chapters these processes are described in more detail.

2.2   Horizontal domain

The default domain of LOTOS-EUROS is shown in Figure 2-1. The boundaries of this domain are 35 and 70 North and 15 West and 35 East. As long as input data is available, the size and position of the domain can be changed. LOTOS-EUROS interpolates input data, if needed.

2.3   Horizontal resolution

The standard grid resolution is 0.50° longitude × 0.25° latitude at a rectangular and regular longitude-latitude grid (at 50° North about 36 km x 28 km). The resolution can be changed to obtain a higher resolution; zoom factors of 4 to 5 are feasible, and preferably the grid matches the emission grid. It is also possible to simulate on non-Cartesian grids, e.g. matching the grid of the meteorological driver. Note that this is only useful, if input data is available on the higher resolution. It is not recommended to use the current versions for horizontal resolutions below 2 km.
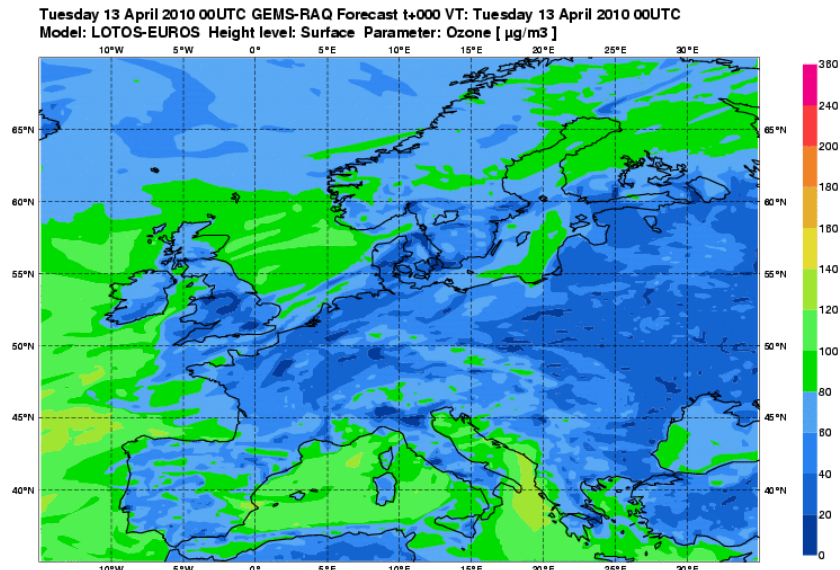
Figure 2-1   The default domain of the LOTOS-EUROS model.

2.4   Vertical layers

From v2.2 onwards, there are several options for the vertical structure of the model. The default option is to calculate directly on the layers of the meteorological model. In order to keep the run time within reasonable bounds, a number of layers of the meteorological model can be combined into single model layers. The current practice is to use 12-15 layers for the troposphere, with higher resolution close to the surface. For details we refer to the user guide, and the best option depend on the exact meterological input data set.

The second option is to calculate on hybrid layers, as used by many meteorological models. By using a fixed definition of these layers, input from several meteorological models can be used in the same way. The benefit of this option is that by defining the hybrid levels, one is not dependent on (changees in) the vertical structure of the meteorological input data. The drawback is that this option may introduce additional vertical interpolations.

The third option was the structure that used to be typical for LOTOS-EUROS, with only a few layers wcih makes the model very efficient in terms of computation time. In the vertical, there are three dynamic layers on top of a constant surface layer. The surface layer has a fixed depth of 25 m and is included to better parameterize surface processes. The model extends in vertical direction 3.5 km above sea level. The lowest dynamic layer is the mixing layer, followed by two reservoir layers. The height of the mixing layer is taken from the meteorological input, usually ECMWF short-range forecasts. New mixing layer heights are read whenever available; for the ECMWF input this is every 3 hours. The model uses linear interpolation within the time interval of 3 hours. The height of the reservoir layers is determined by the difference between ceiling (3.5 km) and mixing layer height (see Figure 2.1). Both layers are equally thick with a minimum of 500 m. In some cases, when the mixing layer extends near or above 3500 m, the top of the model exceeds the 3500 m according to the above mentioned description. In LOTOS-EUROS 2.0, an additional reservoir layer is implemented, which is relevant over areas with high mountains, bringing the model to 5 km. This model version is suitable for calcuations at intermediate resolution and can be a good option for scenario simulations and data assimiliation, however the performance is less good than when using the meteorolagial levells, in particular for high-resolution applications.

For output purposes, a diagnostic layer is used to calculate concentrations near the surface (reference height of 2.5 m). It uses the average concentrations in the lowest layer and calculates a vertical profile due to dry deposition.
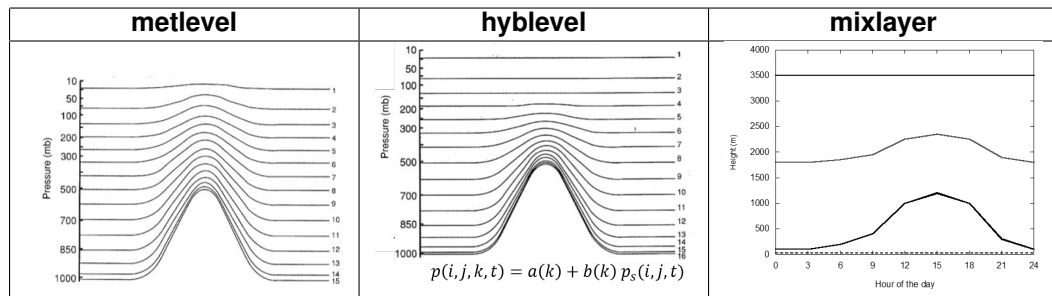
Table 2.1   Illustration of level definitions.

2.5   Simulated tracers

LOTOS-EUROS simulates the concentrations of reactive gases and aerosols in the boundary layer. Simulations for these components are often coupled, but this is not always necessary. For example, one may be interested in ozone but not in aerosols. Therefore, LOTOS-EUROS has the ability to perform simulations of different groups of tracers.

- *Oxidants (default)*
  To calculate ozone and other oxidant levels a gas phase chemistry scheme is used, based on the CBM-IV mechanism. This scheme describes photo-chemistry in about 30 tracers, including ozone, nitrogen oxides, organic compounds, and radicals. The only aerosol species calculated in these schemes is sulphate.

- *Secondary Inorganic Aerosol (default)*
  The SIA simulation invokes a call to the aerosol equilibrium module, which describes the equilibrium between ammonium nitrate and its gaseous counterparts, ammonia and nitric-acid. SIA calculations can only be performed in combination with the full oxidant scheme.

- *Primary aerosol (default)*
  This option enables to switch on/off the calculations for primary aerosol components. At the moment, the primary components include primary PM2.5, PM10-2.5, Elementary Carbon (EC), Particulate Organic Matter (POM), sea-salt, and dust. The calculations for the primary components can be performed stand alone, and could be limited to a selection of the components only.

- *Secondary organic aerosol (optional)*
  This option invokes a call to the aerosol equilibrium module, which describes the formation of secondary organic aerosol (SOA). SOA calculations can only be performed in combination with the full oxidant scheme.

- *Sulphur-only (optional)*
  The sulphur-only option performs a simulation for SO_2 and SO_4 using predefined OH radical concentrations. Hence, the simulation comprises only 2 tracers and is very fast. The sulphur-only option can not be performed together with oxidant calculations, as it was designed to reduce the computational effort by avoiding the full oxidant calculations.

- *Methane-only (optional)*
  The methane-only option performs a simulation for CH4 using predefined OH radical concentrations, similar to the sulphur-only option.

- *Persistent Organic Pollutants (POPs) (optional)*
  LOTOS-EUROS also contains a module to perform calculations for POPs. The code is based on the EUROS-POP module described by Jacobs and Van Pul (1996) and is currently not supported.

- *Heavy Metals (optional)*
  Simulation of lead and cadmium holding aerosols.

- *Base-cat-ions (optional)*
  Simulations of calcium, potassium, magnesium, and sodium content of aerosols released from the soil.

2.6   Time steps

The simulation time steps are set in the following way; see Fig 2-2 for an illustration.

1. The user should specify the 'output' time-step in the settings. A typical value is 1 hour. The model will arrive at every multiple of this output-time-step and put out simulated values.

2. Within an output step, the maximum allowed time step for the individual processes is determined. Currently the advection is the limiting process. The time step limit for advection is based on the CFL-criterion: within a time step, a parcel of air should not cross a complete grid cell, to avoid that some processes are not applied to it. For smaller grid size this leads to a smaller maximum time step; typically, if the resolution in at least one direction doubles, then the number of required time steps is the double too.

3. Within the operator splitting sequence, processes are performed after each other; first all processes in some order for a half the time step, and then in the reverse order for the other half. If a process is to be performed twice directly after each other, the two half-steps are combined into a full-step. In the current operator-sequence the chemistry is the first process and the emission; if three operator splitting steps are required within an output-step, then the emisson is performed three times (full-steps), the chemistry four times (a half step, two full steps, and a half step), and all the other processes six times (six half steps).
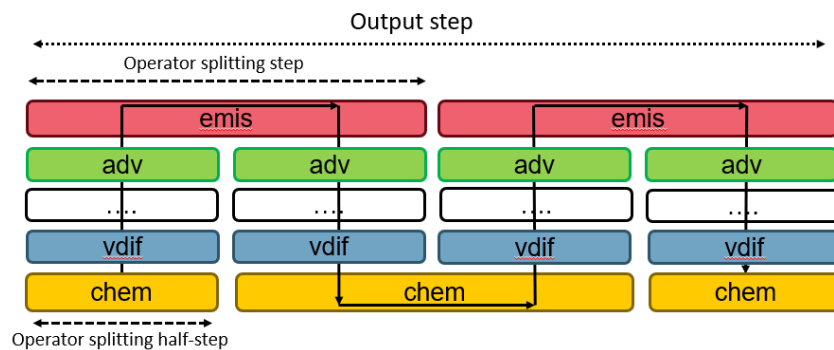
Figure 2-2   Illustration of time step settings.

3   Transport

The transport consists of advection in 3 dimensions, entrainment, and vertical and (optional) horizontal diffusion.

3.1   Advection

In v2.2.009 a new advection scheme was implemented. The goal of the new scheme was to have an advection operator that is potential linear to ensure tracer mass conservation. In addition, the new implementation allows more efficient parallelization and reduced model complexity. The new scheme uses piecewise linear functions to define sub-grid concentrations, which is sometimes referred to as MUSCL (*Monotonic Uwind-centered Scheme for Conservation Laws*) following (Leer 1977).

The implementation is based on movement of air masses over grid cell boundaries, following the method described in (Hooghiemstra 2006). The method is illustrated in figure 3-1. Tracer concentrations in a cell are described by an average value and the linear *slopes* in all directions that describe the inner-cell gradients. At the end of an advection step, the air mass in cell is the result of air masses originating from other grid cells or from what is remaining in the cell; for each tracer, the new average concentration and slopes are obtained as the best fit with the originating concentration distributions.

The advection scheme requires air mass fluxes [kg/s] through all 6 edges of the grid cell. The horizontal air mass fluxes are computed from the horizontal wind vectors (u, v) [m/s], the air density at the edge of the cell [kg/m^3], and the area of the edge surface [m^2]. The vertical air mass fluxes are computed such that the net change of air mass defined by the sum of the incoming minus outgoing fluxes, is exactly the same as the air mass change defined by the change in air pressure, where the later is is part of the meteorological input.

Although in the *operator splitting* scheme (section 2.6) the advection is treated as a single process, the implementation is splitted per direction. Depending on the position of the advection step in the operator splitting scheme, the order of the directions is either xyz or zyx. Eventually also horizontal diffusion operations in x or y directions are included as additional steps (see section 3.2).

The time step of the advection is limited by the ratio between the outgoing air mass flux and the air mass originally present in a cell; the time step should be small enough that at least a small fraction of the air mass remains present.
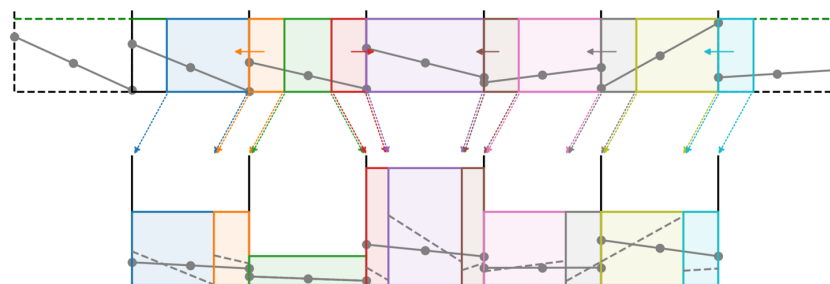
Figure 3-1   Illustration of advection. The air masses at the start of the advection (top row) are transported to a new position; at the end of the advection (bottom row), the new concentration distribution are computed from the originating distributions.

3.2   Horizontal diffusion

Horizontal diffusion was reintroduced in v2.2.003 as for high resolution (higher than 5 km) the concentrations from stacks would be too much aligned with the north-south and east-west directions. In v2.2.009, the operator was re-implemented and integrated with the new advection scheme; the application of the process is controlled by a flag that is by default only enabled for high-resolution grids.

The purpose of the new horizontal diffusion operator is to ensure that simulated plumes have the same width independend of the wind direction. Without additional diffusion, a plume advected in a 45-degree angle is most broad as result of numerical diffusion caused by advection being splitted in x- and y-directions. At 0-degree angles, the numerical diffusion is small however, and plumes remain narrow. To ensure that the plume width is the same independend of the wind direction, horizontal diffusion coefficients (K_x, K_y) have been parameterized as function of wind direction, wind speed, and grid cell sizes. For north- or south-ward wind directions, only the K_x coefficient is non-zero, while for east- or west-ward directions, only the K_y coefficient is non-zero (figure 3-2).
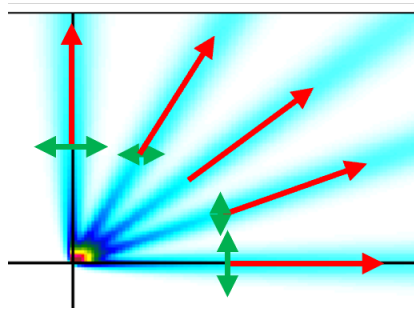
Figure 3-2   Illustration of horizontal diffusion depending on wind direction. Extra diffusion (green arrows) is added when wind directions (red) are more towards north-south or east-west, to ensure that simulated concentration plumes from a point source (blue) have the same width independend of the wind direction.

3.3   Vertical diffusion

Vertical diffusion is described using the standard K_z-theory. The K_z values are calculated within the stability parameterisation described in section 7.4.

3.4   Entrainment

In case the model is defined following the *mixing layer* approach (see section 2.4), an *entrainment* process is applied.

Entrainment is caused by the growth of the mixing layer during the day. Each hour the vertical structure of the model is adjusted to the new mixing layer depth. After the new structure is set, the pollutant concentrations are redistributed using linear interpolation.

4   Chemistry

Ozone is formed in the atmosphere through chemical reactions between nitrogen oxides (NOx) and volatile organic compounds (VOC). Tens of inorganic and hundreds of organic compounds are known to participate in thou-sands of photo-chemical reactions. The explicit treatment of all of these compounds and reactions would be prohibitively complex in an Eulerian-based chemical transport model such as LOTOS-EUROS, especially when such a model is used for long-term (multi-annual) calculations in the framework of regulatory purposes. Since condensation of atmospheric chemistry is required to reach a level of simplification imposed by computational constraints, methods for minimizing the size of a chemical mechanism have been proposed.

A possible way of condensing the inorganic chemistry within photo-chemical mechanisms is through the lumping of species or the lumping of reactions utilizing specific assumptions, e.g. steady state for some radicals. In the lumped structure approach, organic compounds are apportioned to one or more species on the basis of carbon-carbon bond type or on basis of a reactive group (Gery et al. 1989).

The most widely applied mechanism using the lumped structure approach for representing urban photo-chemistry is the Carbon Bond-IV (CB-IV) mechanism. The CB-IV mechanism originally consisted of 81 reactions. It is probably the most widely used mechanism due to its good performance in polluted areas and its relative small number of reactions.

The gas phase mechanisms also describe the photo-chemical formation of sulphuric-acid and nitric-acid, which drive the formation of secondary inor-ganic aerosol. Below we de-scribe the set-up for the CBM-IV scheme as well as the aerosol chemistry.

4.1   CBM-IV

The gas phase photo-chemistry CBM-IV module in LOTOS-EUROS is a modified version of the CBM-IV mechanism by Whitten et al. (1980). The CBM-IV scheme uses nine primary organic species (i.e., species emitted directly to the atmosphere as opposed to secondary organic species formed by chemical reactions in the atmosphere). Most of the organic species in the mechanism represent carbon-carbon bond types, but ethene (ETH), isoprene (ISOP) and formaldehyde (FORM) are represented explicitly. The carbon-bond types include carbon atoms that contain only single bonds (PAR), double-bonded carbon atoms (OLE), 7-carbon ring structures represented by toluene (TOL), 8-carbon ring structures represented by xylene (XYL), the carbonyl group with adjacent carbon atom and higher molecular weight aldehydes represented by acetaldehyde (ALD2), and non-reactive carbon atoms (NR).

Many organic compounds are apportioned to the carbon-bond species based simply on the basis of molecular structure. For example, propane (CH_3-CH_2-CH_3) is represented by three parafinic groups (PAR) since all three carbon atoms have only single bonds; propene (CH_2=CH-CH_3) is represented as one olefinic group (OLE) representing the carbon-carbon double bond, and one PAR representing the methyl group. Some apportionments are based on reactivity considerations, however. For example, olefins with internal double bonds are represented as ALD2s and PARs rather than OLEs and PARs. Further, the reactivity of some compounds may be lowered by apportioning some of the carbon atoms to the non-reactive class NR. For example, the less reactive ethane (C_2H_6) is represented as 0.4 PAR and 1.6 NR EPA (1999). Apportioning rules have been established for many organic compounds and can be found in e.g. Gery et al. (1989) and Carter (1994).

The full mechanism, including the reaction rate parameterisation, is shown in Appendix B. The scheme includes 33 species and 104 reactions, including 14 photolytic reactions. Compared to the original scheme, steady state approximations were used to reduce the number of reactions. In addition, reaction rates have been updated regularly. The mechanism was tested against the results of an inter-comparison study presented by Poppe et al. (1996) and found to be in good agreement with results presented for other mechanisms. The chemistry scheme further includes gas phase and heterogeneous reactions leading to secondary aerosol formation as presented below. The CBM-IV chemistry is solved using the TWOSTEP numerical integration method (implicit, 2nd order, 2-step BDF formula, combined with a simple explicit Gauss-Seidel technique) as described in Verwer et al. (1996).

4.1.1   *Sulphate production*

It is important to give a good representation of sulphate formation, since sulphate is an important aerosol component. In addition, it competes for the ammonia available to combine with nitric-acid. Most models that represent only a direct coupling of sulphur chemistry with photochemistry underestimate sulphate levels in winter in Europe. This feature can probably be explained by a lack of model calculated oxidants or missing reactions (Kasibhatla et al. 1997). Therefore, in addition to the gas phase reaction of OH with SO2 (in CBM-IV) we represent additional oxidation pathways in clouds. The cloud chemistry routine of LOTOS-EUROS calculates a pH-dependent conversion, making using of dissociation and Henry coefficients, cloud cover and cloud liquid water content in a grid cell. Oxidation by O_3 and H_2O_2 are included following the wet phase reactions in Seinfeld and Pandis 2006.

4.1.2   *Heterogeneous N_2O_5 and HNO_3 chemistry*

The reaction of N_2O_5 on aerosol surfaces has been proposed to play an important role in tropospheric chemistry. This reaction is a source for nitric-acid during night time, whereas during the day the NO_3 radical is readily photolysed. This reaction is parameterized following (Dentener and Crutzen 1993). In this parameterisation, a Whitby size distribution is assumed for the dry aerosol. The wet aerosol size distribution is calculated using the aerosol associated water obtained from the aerosol thermodynamics module (see below). The reaction probability of N_2O_5 on the aerosol surface has been determined for various solutions. Reaction probabilities between 0.01 and 0.2 were found (Jacob (2000) and references therein). A study by Mentel et al. (1999) indicates values at the lower part of this range. Therefore, we use a probability of γ = 0.05, which is somewhat lower than the generally used recommendation by Jacob (2000). In the polluted lower troposphere of Europe, however, the hydrolysis on the aerosol surfaces is fast, with lifetimes of N_2O_5 less than an hour (Dentener and Crutzen 1993). Therefore the exact value of γ does not determine the results strongly. Due to the limited availability of detailed cloud information, we neglect the role of clouds on the hydrolysis of N_2O_5, which may also contribute to nitric-acid formation. However, due to the very fast reaction of N2O5 on aerosol in polluted Europe, the role of clouds on N_2O_5 hydrolysis is probably less important.

The formation of coarse nitrate by the heterogeneous reaction of HNO_3 with sea salt aerosol is included in the heterogeneous reaction scheme, which also calculates the heterogeneous formation of ammonium sulphate from sulphuric acid, water and N_2O_5 (Wichink Kruit et al. 2012).

4.2   Aerosol chemistry

Semi-volatile aerosol species are species that maintain equilibrium between the aerosol and gas phase. Ammonium nitrate is a well known example, but also organic species can be described as semi-volatile components. Below we specify the methods used to calculate the formation of these components in LOTOS-EUROS.

4.2.1   *Secondary Inorganic Aerosol (SIA): Ammonium nitrate formation*

Two thermodynamic equilibrium modules can be used to describe the equilibrium between gaseous nitric acid, sulphuric acid, ammonia and particulate ammonium nitrate and ammonium sulphate and aerosol water. The two modules are:

- ISORROPIA2 (Nenes et al. 1999; Fountoukis and Nenes 2007); this is the default scheme;

- EQSAM (Metzger 2002); this scheme is faster.

Equilibrium between the aerosol and gas phase is assumed at all times.

4.2.2   *M7 aerosol represenatation*

The model could be configured to use M7 aerosol representation instead of the defaulte fine/coarse representation.

Note that:

- The M7 definition has currently no tracers for:

    - NO_3
    - NH_4
    - secondary organic aerosol

- Emissions should be assigned to a size distribution, current implementation is just a first guess.

4.2.3   *Secondary organic aerosol with VBS approach*

In the Volatility Basis Set (VBS) approach, classes of volatile organic compounds (VOCs) are defined based on the volatility of a set of compounds (Donahue et al. 2006; Donahue et al. 2009). Within each class a fraction of the material is partitioned in the gas phase, and another fraction in the aerosol phase. One keeps track of the amount of material within these classes as well as the phases, taking into account:

1. production from both anthropogenic /biogenic and primary/secondary origin;

2. modifications in volatility due to chemical reactions;

3. partitioning between gas and aerosol phase;

4. deposition processes.

We followed the currently usual approach to define nine volatility classes of logarithmic spaced volatilities. The volatility of a class of compounds is determined by its 'C* value' (in μg/m^3), which is defined as the concentrations for which half of the material is in the gas phase and half is in the aerosol phase, at default temperature of 313 K. The classes we used vary from C* values of 10^{-2} to 10^6 $\mu g/m^3$ (based on 298 K) representing SVOCs and IVOCs (semi-volatile and intermediate-volatility compounds). For each vbs class, there is a condensable gas and an aerosol part . The total amount of soa and cg is also accumulated as a tracer.

Until now it was assumed in LOTOS-EUROS that Primary Organic Matter (POM) emissions are static, i.e., emission occurs directly in aerosol form and never changes phase. There is evidence that a large part of this POM quickly evaporates, such that a substantial amount of anthropogenic emissions is missed (e.g., Robinson et al. (2007)). The evaporated emissions may later move into the aerosol phase. Thus, we now assume that the POM emissions are distributed over the nine VBS classes. Shrivastava et al. (2008) suggested a division of fractions of POM in the VBS classes.These fractions sum to 2.5, so this means that the total emissions are considered to be 2.5 times higher than the POM emissions in the emission inventory, yet the extra material does not necessarily all end up in the aerosol. When the additional material does end up in the aerosol, this typically occurs after aging, and therefore further away from the source. In our approach, the sum of the four lowest volatilty classes equals the mass that was originally put in the POM tracer. An additional 1.5 times as much mass is put into the higher volatily bins, available to end up as aerosol after aging. Shrivastava et al. (2008) suggest to put more into the higher volatility bins and less in the lower volatily bins, but this yielded less mass in the aerosol phase than the original approach, and we argue that we should reproduce at least the mass of the primary aerosol as reported in the emission inventory.

Additional mass comes from isoprene and terpenes. Biogenic SOA and condensable gases is treated separately from those from anthropogenic origin, since aging yields are different. Not taking this into account would lead to overestimation of the contribution of terpenes to SOA. This implies that for the lowest 6 volatility classes separate tracers are used. Aging rates are still set to conservative values, leading to a limited amount of additional SOA from biogenic origin.

A detailed description of the approach is given in Appendix C. It includes the partitioning formulation, yields for SOA precursors (high-NOx and low-NOx) and description of aging.

5   Dry deposition

This chapter gives a description of the approach for dry deposition of gases and particles. It consists of the following parts:

- treatment of deposition of gases. The DEPAC module that is used is extensively described in a technical report (Zanten et al. 2010) and only key elements will be summarized here.

- parameterization of deposition of particles, which follows the parameterisation by Zhang (2001).

- desrciption of computation of concentrations at measurement height Due to deposition the concentrations at measurement height are slilghty different than concentrations at the first model level.

The basic approach for both gases and particles is that the dry deposition flux F is proportional to the local concentration χ_a at some reference height

$$F = -V_d \chi_a \tag{5.1}$$

with V_d the deposition velocity (or exchange velocity). It is usually determined from a resistance approach and must be defined with respect to the height for which χ_a is defined. Expressions for V_d will be presented in the following sections.

5.1   Surface-atmosphere gas exchange of gases

In the DEPAC module, the exchange of gas between the earth surface and the atmosphere is parameterised using the well-known resistance approach, where the exchange flux is the result of a concentration difference between atmosphere and earth surface and the resistance between them. Several pathways exist for this flux, each with its own resistance and concentration. In DEPAC three pathways are taken into account:

- through the stomata (subscript s)

- through the external leaf surface (water layer or cuticular waxes, subscript w)

- through the soil (subscript $soil$).

It is assumed that ammonia is present in the vegetation, water surfaces and soils, being a potential for emission under certain atmospheric conditions, while in the previous version the concentrations at the surface were zero. DEPAC is prepared to treat other gasses in a similar way, but currently, this compensation point approach is only applied for ammonia. Therefore, the following description mainly concerns the surface-atmosphere exchange of ammonia.

The concentration in the stomata, at the external leaf surface or at the soil surface is for historic reasons called a compensation point. A schematic representation of concentrations χ, resistances R and fluxes F is given in Figure 5-1.

A glossary of terms is given in Table 5.1.

In the text below, we distinguish between upper case and lower case characters: r: leaf resistance; R: canopy averaged resistance; g: leaf conductance = $1/r$; G: canopy averaged conductance $G = 1/R$. For the external leaf conductance, $G = SAI \times g$, with $SAI =$ surface area index (i.e. the area of leaves, branches and stems per unit area of ground surface). For the stomatal conductance, $G = LAI \times g$, with $LAI =$ leaf area index (i.e. the area of leaves per unit area of ground surface).

Table 5.1   List of parameters used in DEPAC

parameter name	units	name in DEPAC	description
χ_a	$\mu g/m^3$	catm	concentration in air
χ_c	$\mu g/m^3$	cc	concentration at canopy top
χ_w	$\mu g/m^3$	cw	concentration at external leaf surface
χ_{soil}	$\mu g/m^3$	csoil	concentration at soil surface
χ_s	$\mu g/m^3$	cstom	concentration in stomata
R_a	s/m	ra	aerodynamic resistance
R_b	s/m	rb	quasi-laminar layer resistance
R_w	s/m	rw	external leaf surface or water layer resistance (also called cuticular resistance)
R_s	s/m	rstom	stomatal resistance
R_{inc}	s/m	rinc	in canopy resistance
R_{soil}	s/m	rsoil	soil resistance
$R_{soil,eff}$	s/m	rsoil_eff	effective soil resistance = $R_{inc} + R_{soil}$
R_c	s/m	rc_tot	canopy resistance
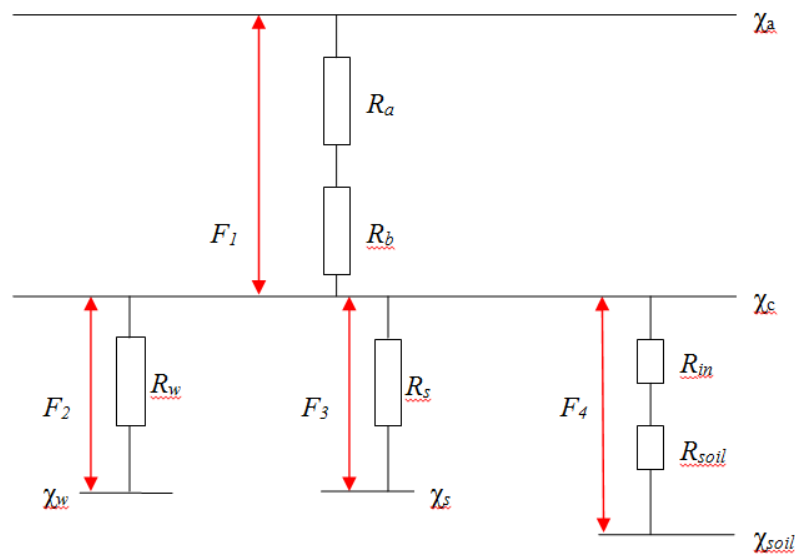
Figure 5-1   Schematic representation of resistance approach with compensation points.

The fluxes F over the different pathways in Figure 5-1 are:

$$F_1 = -\frac{(\chi_a - \chi_c)}{R_a + R_b} \tag{5.2}$$

$$F_2 = -\frac{(\chi_c - \chi_w)}{R_w} \tag{5.3}$$

$$F_3 = -\frac{(\chi_c - \chi_s)}{R_s} \tag{5.4}$$

$$F_4 = -\frac{(\chi_c - \chi_{soil})}{R_{soil,eff}} \tag{5.5}$$

In Zanten et al. (2010), the following expression for the flux F_1 is derived:

$$F_1 = -V_e \ (\chi_a - \chi_{comp}) \tag{5.6}$$

Table 5.2   Landcover types in DEPAC deposition scheme.

class	landcover type
1	grass
2	arable land
3	permanent crops
4	coniferous forest
5	deciduous forest
6	water
7	urban
8	other
9	desert

where the *exchange velocity* is defined by:

$$V_e \;=\; \frac{1}{R_e} \;=\; \frac{1}{R_a + R_b + R_c} \tag{5.7}$$

which uses the *canopy resistance*:

$$R_c \;=\; \left(\frac{1}{R_w} + \frac{1}{R_{soil,eff}} + \frac{1}{R_s} \right)^{-1} \tag{5.8}$$

and the *total compensation point* concentration:

$$\chi_{comp} \;=\; \frac{R_c}{R_w}\,\chi_w \;+\; \frac{R_c}{R_{soil,eff}}\,\chi_{soil} \;+\; \frac{R_c}{R_s}\,\chi_s \tag{5.9}$$

The mass balance in a layer with height H is:

$$H\,\frac{\partial \chi_a}{\partial t} \;=\; F_1 \;=\; -V_e\,(\chi_a - \chi_{comp}) \tag{5.10}$$

If we assume a constant value of χ_{comp} (large reservoir) on a time interval $[t, t + \Delta t]$, we get as solution:

$$\chi_a(t + \Delta t) \;=\; \chi_{comp} \;+\; (\chi_a(t) - \chi_{comp})\,\exp\left(-\frac{V_e}{H}\,\Delta t \right) \tag{5.11}$$

In Zanten et al. (2010) the parameterisations of the different resistances that contribute to the canopy resistance R_c for dry deposition of SO$_2$, NH$_3$, O$_3$, NO, NO$_2$ and HNO$_3$ are described. Resistance parameterisations are different for different land use types. The landcover types used in DEPAC are listed in Table 5.2 (see also chapter 9 on landuse types).

As of version v2.3 also climate zones are implemented for the stomatal resistance, to account for the fact that temperature and vapor pressure deficit parameters that determine this resistance are depending on the climate zone. Before, values representative for temperate zones were used. As one of the most significant examples this leads to and equal stomatal behaviour of boreal and mediterenean coniferous trees. This was considered as one of the reasons for summer time ozone overestimations in mediterenean regions. The climate zone specification is based on Köppen-Geiger (Beck et al. 2018) and available for download at https://www.gloh2o.org/koppen. The parameterisations for mediterenean vegetation were collected from the DO$_3$SE model (Mills et al. 2017).

For the deposition of ozone, the definitions by Simpson et al. (2007) are followed.

Parameterisations of R_a and R_b are not included in DEPAC and are calculated elsewhere. For R_a, one is referred to section 7.5. The leaf-level quasi-laminar boundary layer, R_b, is taken from McNaughton and Van Den Hurk (1995), who use the cross-wind leaf dimension L_d and the wind speed at canopy top (height h), $V(h)$,

$$R_b \;=\; 1.3 \times 150 \times \sqrt{\frac{L_d}{V(h)}} \qquad [\text{s/m}] \tag{5.12}$$

Table 5.3   Particle diameter for dry deposition., PPM = primary particulate matter, BC = black carbon, EC = elemental carbon, OC = organic carbon.

Size category	Indication	species	$D_p(\mu m)$
Very fine	_ff	dust, Na	0.33
Fine	_f	BC/EC, OC/POM, PPM, SO4a, NO3a, NH4a, SOA dust, Na SOA, Ca, Cd	0.70
Finest coarse	_ccc	dust, Na	3.00
Medium coarse	_c	dust, Na	5.00
Coarse	_c	C/EC, OC/POM, PPM, SO4a, NO3a, , SOA dust, Na SOA, Ca, Cd	8.00

The factor 1.3 accounts for the differences in diffusivity between heat and ozone. $V(h)$ is the wind speed at the top of the canopy and is calculated from the standard similarity functions for momentum (in the `le_stability.f90` routine). L_d is set to 0.02 m for land use classes arable and permanent crops and to 0.04 m for deciduous and coniferous forest. For other land use classes, L_d and consequently R_b is 0. The external leaf surface resistance or cuticular resistance, R_w, the soil resistance R_{soil} and the stomatal resistance R_{stom} are described in Zanten et al. (2010).

5.2   Dry deposition of particles

For the dry deposition of particles, the land-use dependent deposition scheme of Zhang (2001) has been implemented in LOTOS-EUROS since v1.8. This scheme is used for its flexibility. Moreover, the formulations have a uniform structure for all land-use classes and an explicit dependence on aerosol size. Furthermore, the scheme formulations compare well, and within validity ranges, with other existing formulations. This scheme can take the size of aerosol into account. In reality, the size is dynamical and depends on the relative humidity. However, for simplicity it is assumed constant for the size categories, which are currently used in LOTOS-EUROS. The applied particle diameters are given in Table 5.3. For particles that are part of emission inventories, only the fine and coarse fraction are defined, as the emission inventories do not provide more detail. For dust and sea salt the emissions are calculated on-line and five size classes are used.

For particles, the pathways are slightly different than for gasses and the *deposition velocity* V_d is characteristized by the gravitational settling velocity V_s, the aerodynamic resistance R_a and the surface resistance R_s following:

$$V_d \;=\; V_s \;+\; \frac{1}{R_a \;+\; R_s}$$ (5.13)

where V_s is mainly relevant for the larger particles. The formulations for V_s and R_a are well established, and based on physical processes. The formulation for R_s is empirical with parameters that are based on a few field studies.

The gravitational settling velocity is determined by the density of the particle ρ, the particle size D_p, the gravitational acceleration g, the Cunningham correction factor C and the viscosity coefficient of air η

$$V_s \;=\; \frac{\rho \, D_p^2 \, g \, C}{18 \, \eta}$$ (5.14)

Zhang (2001) use the following equation for the surface resistance R_s:

$$R_s \;=\; \frac{1}{\epsilon_0 u_*(E_B + E_{IM} + E_{IN})R_1}$$ (5.15)

where ϵ_0 is an empirical constant which is set to 3. The E's are the collection efficiencies for Brownian diffusion, impaction and interception respectively. Factor R_1 is the correction factor representing the fraction of particles that stick to the surface.

The collection efficiency for Brownian diffusion depends on the ratio between the kinematic viscosity of air ν_{air}, and the diffusivity of the particles in air D_{mol}, the Schmidt number S_c, as follows:

$$
\begin{aligned}
E_B &= S_c^{-\gamma} \\
S_c &= \nu_{air}/D_{mol}
\end{aligned}
$$

(5.16)

(5.17)

where the exponent γ reflects the vegetation type.

The impaction efficiency E_{IM} is determined by the Stokes number S_t, a parameter α which depends on the vegetation type, and an exponent β which is set equal to 2. There are two parameterisations for the Stokes number, one for smooth surfaces and one for vegetated surfaces with A being the characteristic radius of the collectors.

$$
E_{IM} = \left(\frac{S_t}{\alpha + S_t} \right)^{\beta}
$$

(5.18)

with

$$
S_t = \begin{cases} \frac{V_g u_*}{g A} & \text{vegetated} \\ \frac{V_g u_*}{g\, \nu_{air}} & \text{smooth} \end{cases}
$$

Note that in the parameterization of the 'smooth' Stokes number the division by g is missing in Zhang (2001). For the original formulas, see Giorgi (1988) for smooth surfaces and see Slinn (1982) for vegetated surfaces.

The interception efficiency E_{IN} depends on the particle diameter D_p and the radius of the collectors A:

$$
E_{IN} = \frac{1}{2} \left(\frac{D_p}{A} \right)^2
$$

(5.19)

Note that E_{IN} as given here, is not applicable for smooth surfaces like sea, ice and desert.

Larger particles may rebound after hitting the surface, a process that depends on the surface type and can therefore be related to the Stokes number S_t. The following parameterisation for the fraction of particles that stick to the surface R_1 is used:

$$
R_1 = \exp(-S_t^{1/2})
$$

(5.20)

For wet surfaces, all particles stick to the surface and R_1 is 1. Values for A, α and γ can be found in Appendix A. In fact A should be dependent on the season, but given the margins of the values in literature this was not implemented.

5.3   Diagnostics at measuring height

The LOTOS-EUROS system contains the option to diagnose the concentration at measuring height z_m (typically 2.5 m). This concentration is lower than the 'atmospheric' concentration in the model layer if dry deposition is active (downward flux through the surface). The concentration might also be higher in case dry emission from the soil reservoir is present, which is currently only taken into account for ammonia; other emissions (upward fluxes through the surface) are not supported yet.

To diagnose the concentration at measuring height, χ_m, we use that the deposition flux is constant over height. Following equations (5.6) and (5.7) for deposition of gasses the flux is related to the 'atmoshperic' concentration χ_a at height z_a (typically the height of the first

layer, e.g. z_a=25m) through the *exchange velocity* V_e, also written as the inverse of the *exchange resistance* R_e:

$$F_1 = -V_e (\chi_a - \chi_{comp}) = -\frac{1}{R_e} (\chi_a - \chi_{comp}) \tag{5.21}$$

A tracer molecule at the measurement height z_m has to overcome less atmospheric resistance to be deposited than a molecule at the height z_a. Following the notations in section 7.5 we describe the 'missing' atmospheric resistance between z_m and z_a as:

$$R_a(z_m, z_a) \tag{5.22}$$

The resistance between measurement height and soil is then:

$$R_e - R_a(z_m, z_a) \tag{5.23}$$

The deposition flux at z_m remains F_1, but could now be written in terms of the measurement concentration χ_m and the remaining resistance:

$$F_1 = -\frac{1}{R_e - R_a(z_m, z_a)} (\chi_m - \chi_{comp}) \tag{5.24}$$

Combining the two expressions for F_1 gives:

$$\frac{\chi_m - \chi_{comp}}{R_e - R_a(z_m, z_a)} = \frac{\chi_a - \chi_{comp}}{R_e} \tag{5.25}$$

which gives an expression for the concentration at measurement height:

$$\chi_m = \chi_{comp} + \frac{R_e - R_a(z_m, z_a)}{R_e} (\chi_a - \chi_{comp}) \tag{5.26}$$

$$= \chi_{comp} + [1 - V_e R_a(z_m, z_a)] (\chi_a - \chi_{comp}) \tag{5.27}$$

The later form is chosen because the exchange velocity V_e is available already for computation of the deposition flux, and the atmospheric resistance over the interval $[z_m, z_a]$ could be evaluated as meteorological variable.

An equivalent expression could be derived for the concentration of particles at measurement height, which is now expressed in terms of deposition velocity V_d and settling velocity V_s following Eq. (5.13):

$$\chi_m = \chi_{comp} + [1 - (V_e - V_s) R_a(z_m, z_a)] (\chi_a - \chi_{comp}) \tag{5.28}$$

6   Wet deposition

Wet deposition consists of the processes of in-cloud scavenging and below-cloud scavenging. In previous versions of LOTOS-EUROS only below-cloud scavenging was included and cloud height was not taken into account (following EMEP scheme). In the current version also a scheme that takes both in-cloud and below-cloud scavenging into account (following CAMx approach, this is now the preferred option). Hence, below we describe the parameterisations for below-cloud scavenging first and then come to the description of in-cloud scavenging.

6.1   Formalism for below-cloud scavenging

For the description of wet deposition a scavenging coefficient Λ [s^{-1}] is used which describes the rate of mass transfer of a contaminant from air into rain droplets. The value of the scavenging coefficient depends on the considered component. However, in general the decrease in the concentration C [μg/m^3] of a component in a time-step t [s] is calculated like:

$$\frac{\partial C}{\partial t} = -\Lambda C \iff C = C_0 e^{-\Lambda t}.$$

(6.1)

Here C_0 is the initial concentration. The contribution to the wet deposition flux ΔD [μg/m^2] in a time step t is calculated as:

$$\Delta D = C_0(1 - e^{-\Lambda t})\Delta z$$

(6.2)

with Δz [m] the height of a grid cell.

6.2   In-cloud scavening

Now that meteorological models that serve as input for chemistry-transport models provide cloud height it is possible to take in-cloud scavenging into account. We use the approach described in Banzhaf et al. (2012) that was based the approach of CAMx (ENVIRON 2010) which relies on formulations as given in Seinfeld and Pandis (2006). In this approach wet deposition is integrated throughout the column. Moving layer by layer downwards, from the layer of cloud top to ground level the loss of material (i.e. the scavenged material) of each layer is transported by the droplet to the layer below. The equations given below are applied for each model level. In-cloud scavenging is dependent on the cloud liquid water content and cloud water pH.

The gas in-cloud scavenging coefficient $\lambda_{icg} = \lambda_{aq} + \lambda_g$ consists of a factor for the aqueous phase scavenging λ_{aq} [1/s] and a factor for scavenging of ambient gases $\lambda_g[1/s]$ (Seinfeld and Pandis 2006; ENVIRON 2010).

$$\lambda_{aq} = \frac{4.2 \times 10^{-7} \cdot E_c \cdot P \cdot H^*(T, pH) \cdot c_g \cdot L_c}{d_d \cdot c \cdot \rho_w}$$

(6.3)

$$\lambda_g = 1.67 \times 10^{-6} \frac{K_c \cdot P}{d_d \cdot v_d}$$

(6.4)

with

$$c = c_g + c_{aq}\frac{L_c}{\rho_w}$$

(6.5)

$$H^*(T, pH) = \frac{c_{aq}}{c_g} \tag{6.6}$$

The coefficient λ_g depends on s the collection efficiency for precipitation collecting cloud droplets (E_c), the precipitation rate at ground level P [mm/h], the effective Henry's law coefficient $H^*(T, pH)$, the gas concentration and the aqueous concentration of a species, the total grid cell concentration, the cloud water content L_g The coefficient λ_g depends on the drop diameter d_d [m] , the water density, the mass transfer coefficient K_c [m/s] and the mean drop fall speed v_d [m/s].

Since below the cloud the ambient gas is subject to scavenging the below-cloud scavenging coefficient λ_{bcg} is equal to λ_g . The equation for λ_g accounts for the mass transfer of ambient gases to the droplet surface and can be used to calculate the scavenging of very soluble gases for which the scavenging is irreversible. To consider gases with low solubility and reversible scavenging, droplet saturation is incorporated for gas wet scavenging by calculating the maximum possible gas in solution c_{eq} as a function of pH. Rainwater pH is calculated on each model level as described above.

The change in gas concentration Δc is given by:

$$\Delta c = (c_{eq} - c_0) \cdot (1 - \exp(-\lambda_{icg/bcg} \cdot \delta t)) \tag{6.7}$$

Δc is relaxed towards the difference between the maximum possible gas in solution for the given conditions and the amount of pre-existing gas in solution from layers above c_0 (ENVIRON 2010). The equilibrium gas concentration $c_e q$ is calculated by means of the effective Henry's law coefficient $H^*(T, pH)$, the pre-existing gas in the droplet solution c_0 and the applied time step. The change in gas concentration Δc can be either positive or negative. In this way, aqueous equilibrium between ambient gas and precipitation is not assumed as a consequence of the relatively short residence times of falling precipitation through a given grid cell.

Banzhaf et al. (2012) performed some sensitivity experiments for the impact of pH-dependency of SO_2 and NH_3 deposition. For high pH the effective Henry's law coefficient $H^*(T, pH)$ for SO_2 is very high (Seinfeld and Pandis 2006). Hence, most available SO2 dissolves into cloud water, SO_2 gas concentration moves towards zero and the gas in-cloud scavenging coefficient stops increasing with increasing cloud water pH and so does the SO_2 wet deposition flux. The opposite behavior can be observed for NH_3 since the effective $H^*(T, pH)$ for NH_3 decreases with increasing pH. Thus, NH_3 wet deposition increases with decreasing droplet pH and converges to a maximum of about $0.9 \cdot 10^4$ mg/m^2 for the applied set up.

For the scavenging of particles it is assumed that within cloud layers all aerosols exist within the cloud water. Thus the particle in-cloud scavenging coefficient λ_{icp} [1/s] is:

$$\lambda_{icp} = \frac{4.2 \times 10^{-7} E_c \cdot P}{d_d} \tag{6.8}$$

with E_c the collection efficiency for precipitation collecting cloud droplets. The particle below-cloud scavenging coefficient λ_{bcp} [1/s] is expressed by:

$$\lambda_{aq} = \frac{4.2 \times 10^{-7} E_p \cdot P}{d_d} \tag{6.9}$$

with E_p the collection efficiency for particles. E_p is a function of the particle diameter the kinematic viscosity of air and water and the ratio of particle size to hydrometer size (Seinfeld and Pandis 2006; ENVIRON 2010).

Table 6.1   Overview of below cloud scavenging coefficients for gases

Component	$\Lambda_{bc} \times 10^6 s^{-1})$
SO2	0.15
HNO3	0.5
NH3	0.5
H2O2	0.5
HCHO	0.05

6.3   Approach with simple below-cloud scavenging coefficients

In older versions of LOTOS-EUROS, scavenging of gases and aerosols was described with below-cloud scavenging only. The advantage of this method was that no 3-D cloud information was needed. The option is still there in the code but the method described above is more accurate. The scavenging coefficient Λ_p [s^{-1}] for below-cloud scavenging of aerosols in LOTOS-EUROS is described in the same way as in older versions of the unified EMEP model, based on Scott (1978):

$$\Lambda_p = \frac{A \cdot P}{V_{dr}} \overline{E} \tag{6.10}$$

Here the empirical coefficient A = 5.2 m^3/kg/s, the raindrop fall speed V_{dr} = 5 m/s and P is the precipitation rate in kg/m^{-2}/s (which is the same amount as in mm/s). Finally, $\overline{E}$ [-] is the size-dependent collecting efficiency of aerosols by the raindrops, which equals 0.1 for the fine mode and 0.4 for the coarse mode. As an example, consider a rain event which lasts for 1 hour and yields a total of 10 mm of precipitation, which equals P = 0.0028 mm/s. Using the equation above, one obtains Λ_p = 0.00029 s^{-1} which in turn corresponds with a timescale of approximately 1 hour (= $1/\Lambda_p$).

Below-cloud scavenging of gases is described as:

$$\Lambda_g = \frac{\Lambda_{bc} \cdot P}{\Delta z \cdot \rho_w}. \tag{6.11}$$

Here Λ_{bc} is a component dependent wash-out coefficient which typically ranges between 10^5 and 10^6 s^{-1} (Table 6.1), P is again the precipitation rate in kg/m^{-2}/s, Δz is the scavenging depth taken equal to 1000 m and ρ_w is the water density (1000 kg/m^3). Using these last two values, the scavenging coefficient Λ_g depends only on precipitation rate P and a component-dependent value for Λ_{bc}. Taking $\Lambda_{bc} = 10^6$ s^{-1}, one gets Λ_g = 0.00028 s^{-1}, which corresponds (like in the case of aerosol scavenging) to a typical timescale of 1 hour.

7 Meteorology

The LOTOS-EUROS model uses off-line meteorology. Meteorological fields are read from files with time series of data at for example 3 hourly resolution.

The storage and reading of meteorological fields has been revised completely for OpenLE v1.0 and LOTOS-EUROS v1.10.007. The new implementation is based on general routines that are able to handle data files in NetCDF format following commonly conventions. At introduction of these versions, the only supported data files are retrieved from the ECMWF meteorology using scripts that accompany the model.

Previous versions of the model also supported meteorological data from the RACMO regional climate model and the WRF meteorological model. The new generic interface of the model is able to support data files produced by WRF and COSMO.

The following section describes the meteorological fields currently used and obtained from ECMWF. However, the description for other data sources would be quite similar.

7.1 ECMWF meteorological fields

LOTOS-EUROS reads the netCDF-files that are retrieved from ECMWF. Different data sets are available, see figure 7-1 for an overview. The most commonly used is the Operational Data, since this has to be used for the daily forecasts. In some occasions ERA-Interim is used for early years.
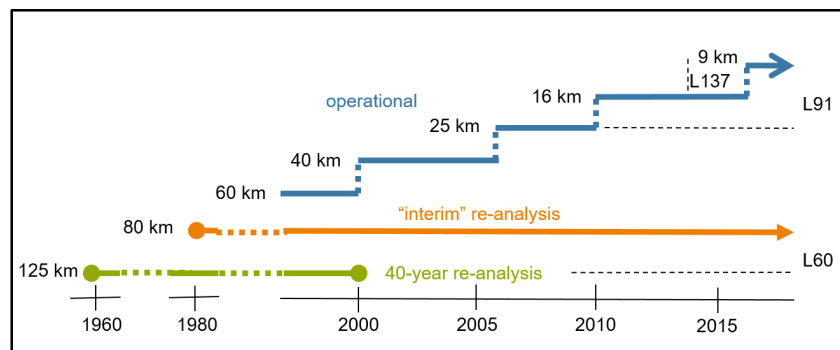
Figure 7-1   Overview of available ECMWF meteorological data.

The following ECMWF model level fields are used (the grib table and parameter id are added in parentheses):

- half level pressure, derived from log-surface-pressure (128.159) and hybride-sigma-pressure coefficient;

- temperature (128.130)

- wind velocity u and v components (128.131, 128.132)

- specific humidity (128.133)

- cloud cover (128.248)

- cloud liquid and ice water content (128.246, 128.247)

The following ECMWF surface fields are used:

- orography (128.129), land/sea mask (128.172), soil type (128.143)

- Boundary layer height (128.159)

- Wind velocity in u and v direction at 10 m (128.165,128.166)

- Temperature and dewpoint temperature at 2 m (128.167,128.168)

- Surface heat fluxes: sensible and latent (128.146, 128.147)

- Friction velocity (228.003)

- Radiation : Surface Solar downward (128.169)

- Total cloud cover (128.164)

- Precipitation: large-scale, convective (128.142, 128.143)

- Snow depth (128.141), snow fall (128.144)

- Sea surface temperature (129.034)

- Sea ice cover (128.31)

- Volumetric soil water content layer 1-4 (128.39-128.42)

Depending on the field, values are interpolated towards LOTOS-EUROS cell centres, edges, full levels or half levels. The ECMWF fields are obtained at a longitude/latitude grid, where the latitudinal spacing could be irregular. Horizontal bi-linear interpolation or area-averaging is applied to map the input to the LOTOS-EUROS grid. The 3D fields are then mapped to the model levels using air-mass weighted averaging. In time, linear interpolation is used to obtain meteorological values at required time steps between the data frequency (3 hourly or less).

7.2   Derived meteorological fields

Some other meteorological parameters are derived from the input:

- grid level altitudes (above sea level) and heights (relative to orography);

- layer thickness and cell volumes;

- grid cell air mass and air density;

- volume fluxes in all 3 directions as required by the advection scheme, vertical flux follows from net horizontal flux and volume change;

- relative humidity;

- total rain (large-scale plus convective), values below 1 mm/hour are ignored to avoid surfaces as marked wetted with impact on dry deposition and dust emission;

- in-cloud coverage, in-cloud liquid water content, below-cloud coverage, over-head cloud coverage;

- rain intensity (3D, derived from 3D in-cloud coverage and 2D total rain);

- soil moisture index, gravimetric soil water;

- friction velocity (section 7.3), stability parameters and vertical diffusion coefficient (section 7.4.2),

7.3   Wind-speed profile

7.3.1   Homogeneous land-use

The wind-speed profile close to the ground is important for deposition and emission of natural dust. We assume a logarithmic wind-speed profile:

$$u(z) = \frac{u_\star}{\kappa} \ln(\frac{z}{z_0}) \quad [\text{m/s}] \tag{7.1}$$

where:

- z_0 [m] is the *roughness length* of the surface;

- $z > z_0$ [m] is the *height* above the surface;

- $u_\star$ [m/s] is the *friction velocity* for the profile;

- κ is the Von Karman constant (0.35).

See illustration in figure 7-2.

The *roughness length* z_0 is assumed based on the land-use type and may depend on the season (arable land). Rougnhnes lengths for all used landuse types are defined in Table 9.1

To obtain the *friction velocity*, the wind speed at a reference height is used. Here we use the 10 m wind-speed from the meteorological input:

$$u(z_{10m}) = u_{10m} \quad [\text{m/s}] \tag{7.2}$$

Given the assumed profile eq. (7.1) and the assumed roughness length z_0 the friction velocity is then:

$$u_\star = \kappa\, u_{10m}\, /\, \ln(\frac{z_{10m}}{z_0}) \quad [\text{m/s}] \tag{7.3}$$
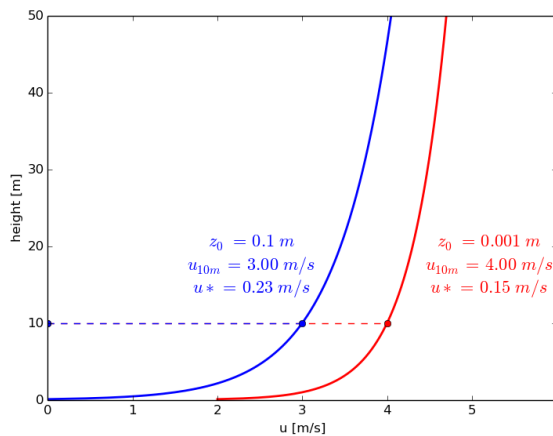

Figure 7-2   Illustration of wind-speed profile for two different roughness lengths. For each profile a wind-speed at 10 m is assumed.

7.3.2   Mixed land-use

The wind-speed profile strongly depends on the roughness length associated to the land-use. A complication in the model is a single grid cell can hold multiple land-use types, each

with a different roughness length. The meteorological input is available with only value per grid cell however, and needs to be downscaled to the different land-use types. Ideally the meteorological model and the chemistry transport model would use the same grid and land use maps. But since this is usually not the case we use a logarithmic average of the contributions of all land use fractions and their roughness length over the grid cell. For most processes the z_0 value per land use class is used but for grid-cell wide processes we use an averaging over the roughness lengtsh per land use class. The approach by Agterberg and Wieringa 1989 is taken, with $z_r = 60$ m **for stability 50 m taken** the refenrence height, κ the Von Karman constant and Cd the drag coefficient:

$$z_0 = z_r \exp\left(\frac{-\kappa}{\sqrt{Cd_{ave}}} \right). \tag{7.4}$$

For the drag coeffcent we take the average of the drag coeffiecnets for the different land use classes according to

$$Cd_{ave} = \sum_i^N \text{fractionalcoverage}_i * \left(\frac{\kappa}{\log(z_r/z_{0i})} \right)^2 \tag{7.5}$$

7.4 Stability and vertical diffusion coefficient

LOTOS-EUROS has several options to determine vertical diffusion across the model layers. One approach is to closely follow the approach taken by ECMWF in its IFS system, which calculates the stability based on heat balance. The alternative (older) approach determines stability based on Pasquill classes, which leads to large steps in the Monin-Obhukov lenght and is less internally consistent. For example, for snow cover the stabilty has to be changed expliclity in the second approach whearas in the first approach it is implicitly accounted for in the surface heat balance. In addition, the Pasquill clases were not intended to be used use above sea surface. However, some artefacts in ozone daily profiles were found when using our implementation of the IFS approach. Therefore the default option is now the approach based on Pasquill class. Both approaches are described here.

7.4.1 IFS approach

The approach follows Chapter 3 of the IFS model documentation (ECMWF 2021). The IFS model iteratively solves the equations, here we use the solutions to the equations. The Monin-Obhukov lenght L is calculated based on the virtual temperature flux in the surface layer, the friction velocity for grass and the 2m-temperature.The Richardson number is claculated from dry static energy, temperature and wind filed and then used to calculate the vertical diffusion across each layer taking into. account the wind speed profile. The IFS scheme puts a limit on z/L to avoid very large values in the similarity functions and unrealistically low vertical exchange. We included this by setting a minimum of $z/L = 10$ which is larger than the IFS implementation ($z/L = 5$).

7.4.2 Exposure class approach

The vertical diffusion coefficient K_z is determined by:

$$K_z = \frac{\kappa u_*}{\Phi\left(z/L\right)} \tag{7.6}$$

Table 7.1   Coefficients for the computation of the Monin-Obhukov length

Pasquill Stability Class	a	b
A (extremely stable)	-0.096	0.029
B (moderately unstable)	-0.037	0.029
C (slightly unstable)	-0.002	0.018
D (neutral)	0	0
E (slightly stable)	0.004	-0.018
F (moderately stable)	0.035	-0.036

Table 7.2   Estimation of Pasquill stability classes.

10 m wind m/s	Daytime without substantial snow and cloud-cover <0.95					Nigthttime or substantial snow or cloud-cover ≥ 0.95		
	Incoming solar radiation [W/m^2]					Cloud cover fraction		
	> 700	$350 - 700$	$125 - 350$	< 125		<0.5	0.50-0.95	≥ 0.95
				$< 12:00$ (sun rise)	$\geq 12:00$ (sun set)			
<2	A	A	B	E	C	F	E	D
2-3	A	B	C	D	D	F	E	D
3-5	B	B	C	D	D	E	D	D
5-6	C	C	D	D	D	D	D	D
>6	C	D	D	D	D	D	D	D

where:
κ	=	von Karman constant (0.35)
u_*	=	friction velocity
z	=	height
L	=	Monin-Obukov length
Φ	=	function proposed by Businger et al. (1971).

The Monin-Obukov length L is determined following Seinfeld and Pandis (2006):

$$\frac{1}{L} = a + b \log z_0 \tag{7.7}$$

with z_0 the surface roughness length with a and b being constants given in Table 7.1. The constants are determined for the different Pasquill stability classes as presented in Table 7.2. A threshold value z_{0thr} is set in the calculation of L, since the values in Table 7.1 were derived for z_0 values smaller than 0.5 and extrapolation to much larger values leads to artefacts.

Stability classes above water are restricted to stable, neutral or slightly unstable. For cases with low zenith angles (incoming solar radiation less than 125 Wm^{-2}) class D is applied, except for surface winds $<2m/2$ for which class E is applied for morning hours and class C is applied for evening hours.

For a stable atmosphere ($L > 0$) the expression of the empirical function Φ is:

$$\Phi_s \left(\frac{z}{L} \right) = 1 + 4.7 \left(\frac{z}{L} \right) \tag{7.8}$$

For an unstable atmosphere ($L < 0$) the expression is:

$$\Phi_u \left(\frac{z}{L} \right) = \left(1 - 15 \left(\frac{z}{L} \right) \right)^{-0.25} \tag{7.9}$$

For a neutral atmosphere the function is equal to unity.

The friction velocity follows from:

$$u_* = \frac{\kappa u_r}{f} \tag{7.10}$$

with u_r being the wind speed at a reference height (10 m) given as input into the model.

The function f in a stable atmosphere is given by:

$$f(z_r) \;=\; \ln\left(\frac{z_r}{z_0}\right) + 4.7\left(\frac{z_r - z_0}{L}\right) \tag{7.11}$$

In an unstable atmosphere the function f is:

$$
\begin{aligned}
f(z_r) \;=\;\; & \ln\left[\frac{1 - \Phi_u\left(\frac{z_r}{L}\right)}{1 + \Phi_u\left(\frac{z_r}{L}\right)}\right] - \ln\left[\frac{1 - \Phi_u\left(\frac{z_0}{L}\right)}{1 + \Phi_u\left(\frac{z_0}{L}\right)}\right] \\
& + 2\tan^{-1}\left(\frac{1}{\Phi_u\left(\frac{z_r}{L}\right)}\right) - 2\tan^{-1}\left(\frac{1}{\Phi_u\left(\frac{z_0}{L}\right)}\right)
\end{aligned}
\tag{7.12}
$$

with the empirical function for an unstable atmosphere Φ_u applied on the reference height z_r and on the height of the surface roughness z_0.

7.5   Aerodynamic resistance

From the stability parameters presented above one can calculate the aerodynamic resistance:

$$R_a(z_0, h) \;=\; \int_{z_0}^{h} \frac{\Phi(z)}{\kappa u_* z}\, dz. \tag{7.13}$$

An evaluation of this integral is:

$$R_a(z_0, h) \;=\; \frac{f_a(h)}{\kappa u_*} \tag{7.14}$$

with f_a analogous to function f, but instead of reference height the integral is taken to the height to which the aerodynamic resistance is required.

8   Emission

The emission module of LOTOS-EUROS describes releases of trace gases and aerosols from various sources. The following emission groups of sources are present by default in the current model:

- anthropogenic sources

- biogenic sources

- sea-spray sources

- dust sources

- forest fires

- special components.

Each of these will be described in detail below.

8.1   Anthropogenic sources

Anthropogenic emissions are a key input to the model. Several sets of emissions are available. By default the MACC emissions are used, that are described in detail here. They cover Europe and its surroundings, including shipping over the Atlantic Ocean. Alternative emission inventories can be used when input is prepared in the right format (e.g. EMEP, EDGAR, MEIC, US EPA, HTAP compilations). In addition to the commonly reported emissions (total PM, SOx, NOx, VOC), special components like heavy metals or base cations can be studied. For these components, separate emission inventories have been prepared but are not updated regularly.

8.1.1   TNO/CAMS inventories

The CAMS and preparing MACC services (www.gmes-atmosphere.eu) are European Union funded projects to operate and improve data-analysis and modelling systems for a range of atmospheric constituents. The project includes a work package on emissions with the objective to update the existing regional emission inventories for Europe and to extend it to cover multiple years. The TNO/CAMS inventories are the result of this work ttps://atmosphere.copernicus.eu/anthropogenic-and-natural-emissions.

The base is formed by a detailed European inventory for 2005 described in Denier van der Gon et al. (2010). By scaling with reported yearly country emissions this inventory was extended to the 2003-2007 (MACC). For MACC-II and MACC-III an update was made (Kuenen et al. 2014), and the most recent version is the TNO/CAMS emission set (Kuenen et al. 2022). The descriptions below belong to the TNO-MACCIII emission set which is currently most widely used. For the TNO-CAMS emissions the changes include a change in category code (GNFR instead of SNAP), a change in resolution (×0.05 degrees longitude × latitude) instead of 1/8 × 1/16 to 0.1) and a change in emission height profile, but the interfaces are similar.

Table 8.1   Source categories in CAMS and MACC emission inventory.

GNFR category	SNAP category	description
A	01.00	Public power stations
C	02.00	Comm inst.combustion
B	34.00	industry
D	05.00	extraction and distribution of fossil fuels
E	06.00	solvents
F	07.00	road transport
F1	07.01	exhaust emissions, gasoline
F2	07.02	exhaust emissions, diesel
F3	07.03	exhaust emissions, other fuels
F4	07.04+07.05	evaporation + road, brake, and tire wear
G,H,I	08.00	other mobile sources (shipping, aviation, other)
J	09.00	waste treatment and disposal
K, L	10.00	agriculture (livestock, other)

8.1.2   Resolution and domain

Emissions are either defined as an area emission or as a point source. An area emission in the current CAMS emissions is valid for a cell in a regular grid with a size of 1/10 degrees longitude by 1/20 degrees latitude, which is about 7 km at European latitudes. Point sources (mainly power plants and large industrial stacks) are given by their actual position (longitude, latitude). The inventory covers Europe up to 60° E, see Figure 8.1. Besides the geographical location, each emission is also assigned to a particular country, or, if this is not possible, to a geographical region (for example "Mediterranean Sea" for ship emissions in this area).

8.1.3   Source categories

The MACC emissions distinguish 13 different source categories (Table 8.1). A category is defined by a sector code and sub-sector code, both identified by 2-digit numbers. Most categories do not distinguish sub-sectors and therefore have sub-sector code 00; only for road transport, 5 different sub-sectors are in use.In sector 8 sometimes shipping is labeled separately as 8.01. For the CAMS emissions, SNAP codes have been replaced by GNFR categories, which are indicated by a combination of letters and numbers.

8.1.4   Emitted components

The inventory quantifies the anthropogenic emissions for in total 8 components (Table 8.2). The first column of the table lists the bulk components that have to be distributed over the available model tracers. The composition of the emitted tracer, and the source of information used to define the composition is listed in the second and third column of the table.

8.1.4.1 NO_x composition

For NO_x emissions, the same composition is assumed for all sources: 3% is emitted as NO_2, and the rest as NO. These fractions are likely to be changed in the near future following the latest insights; the exact composition should be part of the emission inventory.

8.1.4.2   SOx composition

For SO_x emissions, the composition is also constant. By default, 2% is emitted as SO_4 aerosol, the rest as SO_2.

8.1.4.3   NMVOC composition

The emissions of Non-Methane Volatile Organic Compounds are distributed over the model tracers according to the specifications of the chemistry scheme.

The CBM-IV scheme uses nine primary organic species (i.e., species emitted directly to the atmosphere as opposed to secondary organic species formed by chemical reactions in the atmosphere); for more details see the chemistry chapter. The present VOC split (i.e. apportionment of the nine primary VOC species to each emission category) is based on the emission inventory of VOC's, which are specified in 125 different species or classes. These species are translated to Carbon bond species. The total and lumped VOC emissions within an emission category are summed to arrive at the total VOC mass and the total moles of the lumped Carbon Bond species, which were used to determine the average VOC-split for an emission category. For a detailed description we refer to Brouwer (2005).

8.1.4.4   PM composition

The composition of the PM emissions is provided as part of the emission inventory. For a full description see Kuenen et al. (2014). The fraction of EC, POC, SO_4 (a), Na, and remaining PPM is provided as a function of emission category and country. The spatial pattern of the emissions of these components is therefore the same within a country and category, since it is the same as the pattern of the original PM bulk emission. Two PM composition tables are provided, one for the fine fraction (0-2.5 μm) and one for the coarse fraction (2.5-10 μm). As an example, Figure 8-1 shows the total coarse (P)OC emissions derived from the original coarse PM emissions.

Table 8.2   Emitted bulk components and chemical composition for the MACC inventory. The last column describes the origin of the composition.

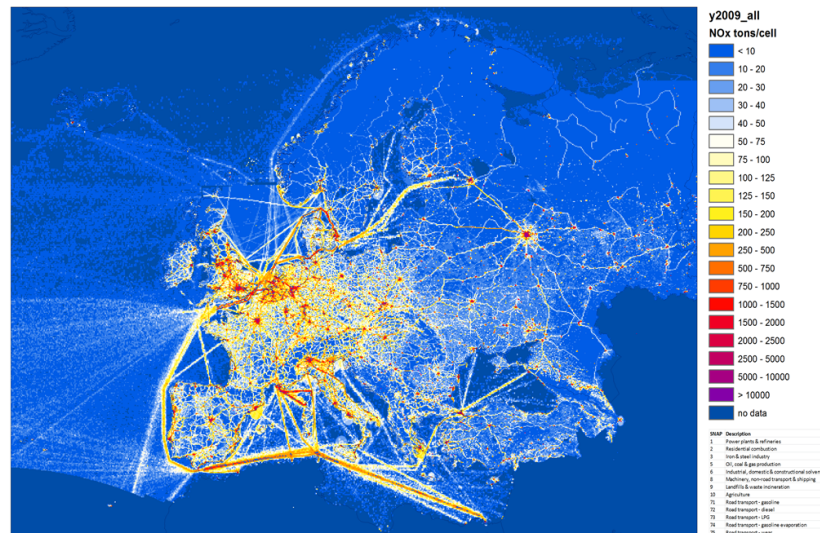| emission	composition	composition table
NO_x	NO, NO_2	3% NO_2
SO_x	SO_2,SO_4 (a)	2% SO_4 (a)
NMVOC	organic compounds	TROTREP (Roemer et al. 2003)
CH_4	CH_4	
NH_3	NH_3	
CO	CO	
PM 0-2.5 μm	EC, OC, SO_4 (a), Na, PPM (0-2.5 μm)	Kuenen et al. (2014)
PM 2.5-10 μm	EC, OC, SO_4 (a), Na, PPM (2.5-10 μm)	Kuenen et al. (2014)

Figure 8-1   Example of spatial distribution of emission in the MACCinventory. The figure shows the NOx emissions in 2009

8.1.5   *Vertical distribution*

Anthropogenic emissions are by default distributed in the vertical, following the profiles defined for the EC4MACS and EURODELTA III project (adapted from Thunis et al. (2008)). Table 8.3 shows the height profiles following this definition. The source categories for solvent use, small combustion sources, transport, and agriculture are always assigned to the lowest model layer. Other sources are distributed over 8 different vertical layers with fixed thicknesses ranging from 90 m for the lowest to 990 m for the top layer. The distribution reflects the average effective injection heights: while power plants emit from high stacks, industrial processes usually emit near the surface. Since the height of the model layers is not fixed but depends on the mixing height, the distribution from the height profile layers to the model layers is re-computed every time step.

Since v.2.2.003, it is possible to include more detailed plume rise information for point sources. With this option it is possible to computes a point-source-dependent and time-dependent effective emission height based on the stack parameters of each point source and the present meteorological conditions. Plume rise due to momentum or buoyancy is considered. Momentum plume rise is calculated following (Briggs 1975), (Turner et al. 1986) which need the diameter of the stack and the output velocity. For the plume rise due to buoyancy the (Briggs 1971) approach is used. Different parameterizations are used for neutral/unstable and stable conditions of the atmosphere. Next, both heights are compared and the higher one is applied to compute the effective emission height for the point source. In the last step, the full emission of the point source is added to the respective model layer. For a full analysis of both plume rise mechanisms (momentum and buoyancy), the following stack parameters need to be defined in the emission input file for each point source :

- source height - stack height [m]

- source diameter - diameter of the stack [m]

- source velocity - exit velocity of plume at stack tip [m s^{-1}]

- source temperature - temperature of effluent from stack [K]

- source volume - volume rate of effluent [m^3 s^{-1}]

If missing stack parameters only allow for the computation of either momentum rise or buoyancy rise, the height of the remaining option is used. If neither option can be calculated due to missing stack parameters it is possible to define the stack height (min. 10 m) as the effective emission height. Next to the stack parameters the following meteorological fields at the location of the point source are used by the algorithm to compute the plume rise height:

- horizonal wind speed at the surface;

- temperature profile;

- Monin-Obukhov length;

- air density;

- surface roughness length.

Table 8.3   Height profiles of emission following EURODELTA definitions.

source category	0-20	20-90	90 - 184	184-324	324 - 522	522-781	781-1106
01 public power stations	-	-	0.25%	51%	54.3%	3.25%	0.2%
02 small combustion sources	100%	-	-	-	-		
34 industry	6%	16.%	75%	3%	-	-	-
05 extraction fossil fuel	2%	8%	60%	30%	-	-	-
06 solvents	100%	-	-	-	-	-	-
07 road transport	100%	-	-	-	-	-	-
08 other mobile	100% -	-	-	-	-	-	
09 waste treatment	-	-	41%	57%	2%	-	-
10 agriculture	100%	-	-	-	-	-	-

8.1.6   *Time profiles*

The basic information, which is also the input data for LOTOS-EUROS, is the gridded yearly averaged anthropogenic emission database. However, in reality, emissions of specific source categories, as for example road transport, depends on whether it is weekend or not and on the hour of the day. Time factors used in the model applied to anthropogenic sources are the result of a review of these factors within the TROTREP project (Roemer et al. 2003). Factors are defined per source category (main sector) for the month in the year, the day within the week, and the hour within the day (Figure 8-2). Note that hour within the day is local time, since it represents features as the rush hour. Information over the deviation from GMT is therefore collected for each country. Currently it is assumed that all countries have the shift from summer to wintertime and vice versa at the same days, i.e. the last Sunday of October and March, respectively. Separate agricultural NH3 emission time profiles that were used in previous versions are no longer used, NH3 emissions now have the same time profile as other agricultural emissions.

Recently, more dynamical time profiles have become available, including heating demand (heating degree days) or cold start emissions. Also country-specific profiles have been produced like CAMS-TEMPO. It is beyond the scope of this reference guide to detail on all available emission time profiles, since it is a rapidly developing area of research and many products are still experimental.

8.1.7   *Temperature profiles*

A temperature-depended factor is applied to emissions of VOC and CO in categories 07.01 (road transport using gasoline), and 07.02 (using diesel). Their emissions are assumed to increase with lower temperatures, as a result of the so-called "cold start". The factors used are shown in Figure 8-3.
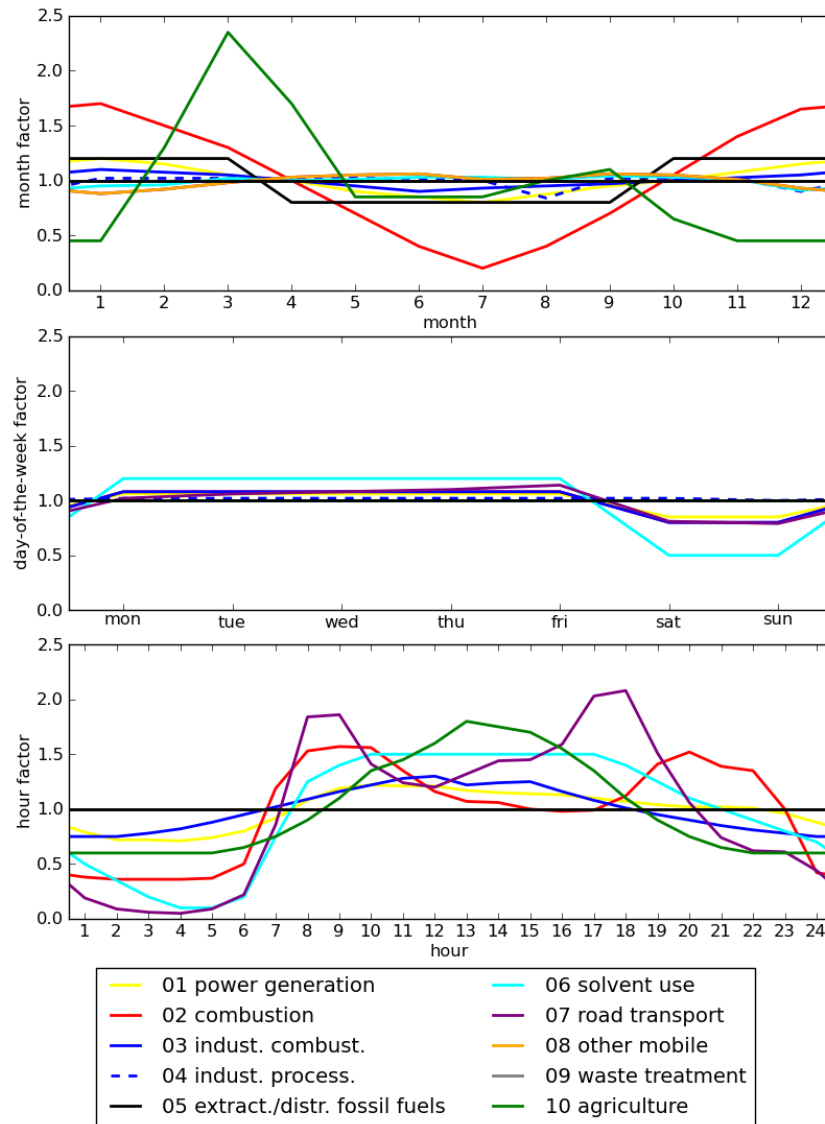
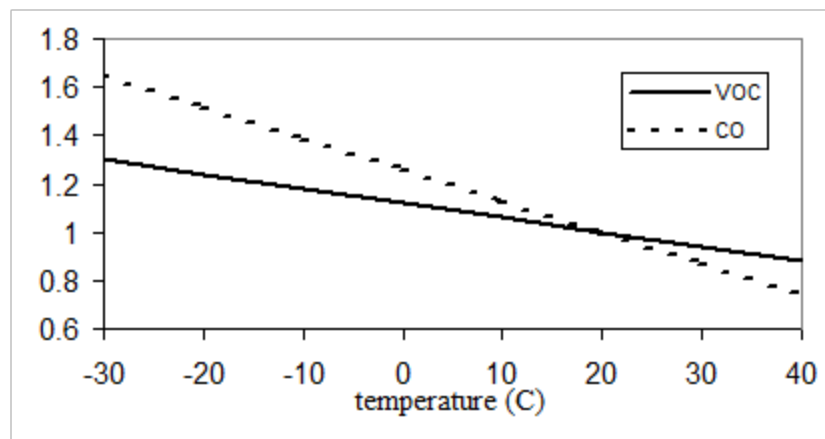Figure 8-2   Time profiles applied to anthropogenic emissions.

Figure 8-3   Temperature factors to be applied for VOC and CO from road transport categories 07.01 (gasoline) and 07.02 (diesel).

8.2　Biogenic emissions using tree species map: isoprene and monoterpene

The biogenic emissions include isoprene and monoterpene from trees, grass, and crops. They depend on temperature, photosynthetically active radiation (PAR) and leaf area index. They are calculated on-line using actual meteorology.

This approach requires a detailed land use and tree species database from Köble, R. and Seufert (2001). This tree species database contains 115 tree species for which biomass density and emission factors for terpene and isoprene are available. Thus, specific emissions per tree species type can be calculated. Coupling of tree species to landuse is described in Chapter 9, tables with tree species and emission factors in Schaap et al. (2009). For areas outside Europe, where not all tree species information is available, the MEGAN biogenic model can be used (section 8.3)

8.2.1　*Isoprene*

All studies on the emission of isoprene and monoterpenes show clear temperature dependence. In addition, isoprene emissions have been shown to be triggered by light, as a result of the link between isoprene emission and syn-thesis from photosynthetic products. As no large isoprene pool exists, synthesis and, hence, emission will cease within minutes under dark conditions (Guenther et al. 1991). For a mathematical description of the temperature and light dependence of the isoprene emissions, empirically designed algorithms are used. One of the commonest algorithms is the formula:

$$E = A \cdot D \cdot ES \cdot \gamma(iso) \tag{8.1}$$

proposed by Guenther et al. (1991) and Guenther et al. (1993), where E is the actual emission [μg/h], A is the area [m^2], D is the biomass density [g/m^2] and ES [μg/g/h] is the standard emission factor per gram dry biomass, per hour (at a standard temperature T_s of 30° C and a standard 1000 μmol/m^2/s photosynthetically active radiation (PAR)). γ(iso) [-] is a function of temperature and light:

$$\gamma(iso) = \frac{\alpha C_{L1} Q}{\sqrt{1 + \alpha^2 Q2}} \cdot \frac{\exp\left[\frac{C_{T1}(T - T_s)}{R T_s T}\right]}{1 + \exp\left[\frac{C_{T2}(T - T_M)}{R T_s T}\right]} \tag{8.2}$$

with:

Q	=	PAR [μmol(photons)/$(m^2 s)$]
T	=	ambient temperature $[K]$
Ts	=	leaf temperature at standard $[K]$ (= $303K$)
R	=	8.314 $J * K^{-1}$mol^{-1}
a	=	0.0027
C_{L1}	=	1.066
C_{T1}	=	95000 Jmol^{-1}
C_{T2}	=	230000 Jmol$^-$1
T_m	=	314 K
C_{T3}	=	0.961.

C_{T2}, T_m, a and C_{L1} are empirically defined parameters, derived from measurements on four isoprene-emitting temperate plant species.

8.2.2　*Monoterpenes*

Monoterpene emissions are generally regarded as light-independent, because monoterpenes are stored after synthesis in special organs, such as resin ducts or glands, exhibiting

quite large storage pools compared to the emission rates (Lerdau 1991; Lerdau and Keller 1997). Hence, their emission, which is temperature-dependent and related to the vapor pressure and to the transport resistance along the diffusion path, is regarded to be a volatilisation out of storage organs (Guenther et al. 1991). The emission response to temperature shows an exponential increase with temperature and is usually described using the formula by Tingey et al. (1980):

$$E = A \cdot D \cdot ES \cdot \exp[\beta(T - T_s)] \tag{8.3}$$

where E [μg/h] is the emission at temperature T [K], A is the area [m^2], D is the biomass density [g/m^2], β is the slope $d(\ln E)/dT$ [K^{-1}], and ES [μg/g/h] is the standard emission factor per gram dry biomass, per hour at a standard temperature, T_s. Values for β found in the literature range between 0.057 and 0.144 K^{-1}. As a generally accepted mean value, 0.09 K^{-1} is used (Fehsenfeld et al. 1992; Guenther et al. 1993).

Some species do not store monoterpenes. For these species the temporal evolution of the emissions is modeled following the above mentioned formulas for isoprene.

8.3   Biogenic emissions using MEGAN

To calculate isoprene and terpene emissions in areas where no tree species information is available and other types of vegetation are found, MEGAN can be used. MEGAN stands for *Model of Emissions of Gases and Aerosols from Nature* and is a modeling system for estimating the net emission of gases and aerosols from terrestrial ecosystems into the atmosphere. Driving variables include land cover, weather, and atmospheric chemical composition.

The current implementation in LOTOS-EUROS is MEGAN v2.04[1]. Input data and source codes are available through the CDP website[2]. The input data was acquired at a resolution of 150sec (1/24 degree).

8.3.1   Plant functional types

One of the base inputs to MEGAN model is a set of maps of the *Plant Functional Type* (PFT). The PFT classifies the vegetation present at a certain location given its properties in relation to biogenic emissions. In this version 4 different PFTs are distinguished (Table 8.4).

Global maps of PFT coverage are provided with the input data. For use in the LOTOS-EUROS model, these maps are regridded to the required model resolution.

---

[1]http://lar.wsu.edu/megan/guides.html
[2]http://cdp.ucar.edu, under '*Models*' select '*MEGAN*'

Table 8.4   Overview of Plant Functional Type (PFT) classes in MEGAN

PFT	description
PFT	description
BT	Broadleaf Tree
NT	Needle leaf Tree
SB	Shrub
HB	Herbaceous Cover

8.3.2   *Species, component classes, and model tracers*

The MEGAN emission model considers three types of chemical components: emitted species, component classes, and model tracers.

8.3.2.1   *Emitted species*

The MEGAN model computes emission rates for 138 different chemical species. In the remainder we will denote a species by s.

8.3.2.2   *Component classes*

To limit the complexity of the computations, MEGAN also considers 20 component classes. A component class (in the the following denoted by c) could account for a single species (isoprene, methane), but also denote a group (acteones). Many of the emission parameters are specified for the component classes only, since no detailed information is known for all the 138 species.

The source code of the MEGAN model provides tables with properties of species and component classes. For each species s, the corresponding component class index is provided, which we will here denote by c_s.

The fraction for which a species contributes to the emissions for this component class is defined for each of the considered plant-functional-types:

$$\phi_c(s, PFT) \in [0, 1] \tag{8.4}$$

where

$$\sum_{s \in c} \phi_c(s, PFT) = 1 \tag{8.5}$$

8.3.2.3   *Model tracers*

To include the MEGAN emissions in a transport model, the emitted species have to be converted to the model tracers. The source code supplied with MEGAN provides a number for conversions for different schemes. The chemistry in LOTOS-EUROS is of the Carbon-Bond mechanism, and the conversion tables are therefore based on those provided with the MEGAN code to support the CBMZ-mechanism. The most important change concerns addition of an extra 'TERP' tracer to account for mono-terpenes. In the original mapping from the 138 emitted species to the CBMZ tracers the emission of a single monoterpine molecule lead to the introduction of 2 ISOP molecules in the model (monoterpines consists of 2 isoprene units); these are now assigned to single TERP molecules.

8.3.3   *Emission rates*

For a grid cell (x,y) and a species s the emission rate is computed following

$$ER(x, y, s) = EF(x, y, s) \; \Gamma(x, y, s) \; \rho(x, y, s) \tag{8.6}$$

where:

- ER is the Emission Rate in [μg/m^2/hr] ;

- EF is the Emission Factor in [μg/m^2/hr] ;

- Γ is the dimensionless emission activity factor representing the impact of meteorological and other external drivers;

- ρ is a dimensionless factor that represents the extra production and loss related to processes within the plan canopies; in the current version this effect is neglected however (ρ=1)

Each of the components that are used to form the emission rate is discussed in the following sections.

8.3.3.1 Emission factor maps

The MEGAN model could use two different methods to compute an emission-factor map for a certain species.

Emission factors based on plant-functional-types In this method, the emission factors are computed based on plant functional types. The base is formed by a set of standard emission factors defined for each of the considered PFTs for all the component classes:

$$EF_0(c, PFT) \qquad [\mu g/m^2/s] \tag{8.7}$$

The factors are provided with the source code. Combined with the contribution factor of a specie to a representer, and the coverage fraction of the PFT in the grid cell this provides the desired map:

$$EF(x, y, s) \;=\; \sum_{PFT} EF_0(c_s, PFT)\, \phi_c(s, PFT)\, \alpha(x, y, PFT) \tag{8.8}$$

Pre-computed emission factor maps Pre-computed maps of emission factors are also provided with the input data for some of the component classes. For MEGAN v2.0 only for isoprene an emission map is provided.

8.3.3.2 Emission activity factor

The emission activity factor quantifies the impact of meteorological and other temporal varying parameters on the emissions. Three contributions are taken into account, for canopy, aging, and soil moisture:

$$\Gamma(x, y, s) \;=\; \Gamma_{canop}(x, y, s)\, \Gamma_{age}(x, y, s)\, \Gamma_{soilm}(x, y, s) \tag{8.9}$$

In here, the canopy correction factor consists of 3 contributions too, to account for variations due to leaf-area-index, the photolysis dependency, and the temperature dependency:

$$\Gamma_{canop} \;=\; \Gamma_{LAI}\, \Gamma_\rho\, \Gamma_T. \tag{8.10}$$

The different factors are discussed in terms of the required input, for the actual parameterizations we refer to Guenther et al. (2006).

Leaf-Area-Index dependency The leaf-area-index (LAI) quantifies the area of the leafs per area of surface. LAI is therefore a function of the vegetation type (amount of leafs and their shape) and the growing season. Maps of leaf-area-index are provided with the input data for each month in 2003.

Photolysis dependency The photolysis activity factor is parameterized using the *Photosynthetic Photon Flux Density* (PPFD) [W/m^2]. Current meteorological models often provide this parameter directly, or otherwise similar parameters such as Photosynthetic Active Radiation (PAR). The MEGAN code that was used in this project computed PAR from the *Surface Solar Radiation Downwards* (SSRD) however, and for consistency and checking this method is used for the implementation in LOTOS-EUROS too. The parameterization actually required two SSRD fields, the current field as well as a daily average field. A

clear definition of daily average in this context was not found; there we choose to use an *Exponential Moving Average* for hourly values:

$$SSRD_{ema}(t) = \frac{23}{24} SSRD_{ema}(t-1) + \frac{1}{24} SSRD(t) \tag{8.11}$$

Temperature dependency The (species depended) temperature activity factor is parameterized using current surface temperature, and in addition the daily average. Similar as for the radiation dependency the daily average is computed using an *Exponential Moving Average*.

Leaf age dependency The age of a leaf has an impact on the emission, and this is quantified by a leaf-age factor. Since the age of the leaves is not recorded, the parameterization is based on the leaf-area-indices for the previous and the current month.

Soil moisture dependency The soil moisture influenced the growth and therefore the activity of the plants. In the current implementation, this effect is neglected however, and the activity factor for soil moisture is set to one.

8.4 Biogenic emissions: NOx from soil

To get a first order estimate of the contribution of NO emissions from soils a very simple parameterization was included, based on the approach of Novak and Pierce (1993). The emission of NO in $ngNm^{-2}s^{-1}$

$$NO\_emis = A_{NO} \exp(0.071 T_{soil}) \tag{8.12}$$

with A_{NO} an emission factor depending on the soil type and T_{soil} the soil temperature. Soil temperature is calculated from air temperature following using the simple parameterization:

$$T_{soil} = C_1 * T_{air} + C_2 \tag{8.13}$$

with all temperatures in $^\circ C$. The coefficients A_{NO}, C_1 and C_2 are indicated in table 9.1. The coefficients are rather uncertain, in particular for agricultural land. Therefore, for agricultural land the values for grassland and pasture were taken, following Simpson et al. (1995). In LOTOS-EUROS, soil NO emissions only take place for grass land, agricultural land, deciduous and coniferous forest. Soil temperature could in principle also be obtained from the meteorological driver (e.g. ECMWF) but the present approach is taken since it does not require additional meteorological variables and makes the model more flexible towards using different meteorological drivers. The parameterization does not include relevant dependencies on e.g. rain and application of fertilizer and tends to give an underestimation as compared to more recent and detailed approaches, but is only intended to produce a realistic background level.

8.5 Sea salt generation

In general, the sea salt emissions are described with a source formulation that is an empirical relation between the whitecap cover, average decay time of a whitecap, the number of drops produced per square meter of whitecap and the resulting droplet flux dF/dr:

$$\frac{dF}{dr_p} = W(U_{10})\frac{dE}{dr_p} \tag{8.14}$$

where:

$$W(U_{10}) = 3.84 \cdot 10^{-6} \cdot U_{10}^{3.41} \tag{8.15}$$

Table 8.5   Coefficients for the polynomial Ak in the Mårtensson parameterisation for three size ranges k

Interval (μm)	a_0	a_1	a_2	a_3	a_4
$0.020 - 0.145$	$-2.881 \cdot 10^6$	$-3.003 \cdot 10^{13}$	$-2.867 \cdot 10^21$	$5.932 \cdot 10^{28}$	$-2.576 \cdot 10^{35}$
$0.145 - 0.419$	$-6.743 \cdot 10^6$	$1.183 \cdot 10^{14}$	$-8.148 \cdot 10^{20}$	$2.404 \cdot 10^{27}$	$-2.452 \cdot 10^{33}$
$0.419 - 2.800$	$2.181 \cdot 10^6$	$-4.165 \cdot 10^{12}$	$3.132 \cdot 10^{18}$	$-9.841 \cdot 10^{23}$	$1.085 \cdot 10^{29}$

Table 8.6   Coefficients for the polynomial Bk in the Mårtensson parameterisation for three size ranges k

Interval, μm	b_0	b_1	b_2	b_3	b_4
$0.020 - 0.145$	$7.609 \cdot 10^8$	$1.829 \cdot 10^{16}$	$6.791 \cdot 10^{23}$	$-1.616 \cdot 10^{31}$	$7.188 \cdot 10^{37}$
$0.145 - 0.419$	$2.279 \cdot 10^9$	$-3.787 \cdot 10^{16}$	$2.528 \cdot 10^{23}$	$-7.310 \cdot 10^{29}$	$7.368 \cdot 10^{35}$
$0.419 - 2.800$	$-5.800 \cdot 10^8$	$1.105 \cdot 10^{15}$	$-8.297 \cdot 10^{20}$	$2.601 \cdot 10^{26}$	$-2.859 \cdot 10^{31}$

and:

dF/dr	source flux of salt particles per increment of drop radius ($\mu m^{-1} m^{-2} s^{-1}$)
r_p	wet droplet radius (μm)
U_{10}	wind speed at ten meter (ms^{-1})
$W(U_{10})$	surface fraction covered with whitecap
dE/dr	droplet flux per increment of drop radius per unit whitecap ($\mu m^{-1} m^{-2}$).

A large number of formulations for the whitecap coverage and flux per whitecap area exist. Here, we used a combination of two parameterisations. For the whitecap coverage we use the formulation by Monahan and O'Muircheartaigh (1980). For the flux per whitecap area two parameterisations are used: Mårtensson et al. (2003) for the fine fraction and Monahan et al. (1986) for the coarse particles. Since the power-law dependency on U_10 may lead to over-estimations of the production for very high wind speeds, a maximum value of 12.5 m/s was implemented. The obtained total flux per grid cell is scaled with the percentage of sea in the grid cell. LOTOS-EUROS uses sodium (Na) as a tracer for sea salt. To obtain total sea salt a factor 3.26 has to be applied (Seinfeld and Pandis 2006). The parameterizations apply for a salinity of about 35 psu, but some seas are considerable less saline, e.g. the Baltic Sea. For the Baltic sea, Na emissions are reduced by a factor 10 to compensate to the low salinity (around 7 psu) (Manders et al. 2010). The salinity of Black and Caspian sea (around 15 psu) is substantially lower that the 35 psu that is assumed, but no corrections have been applied here, which will result in a small overestimation of sea salt emissions in those areas.

8.5.1   *Mårtensson et al. formulation*

The Mårtensson et al. (2003) parameterisation is considered to be a better fit for the fine aerosol mode. For this reason, it is particularly useful for the study of this fine mode contribution to PM2.5. This formulation was used in LOTOS-EUROS for particles with diameter $D_p < 1 \mu m$ (dry diameter $D_d < 0.5 \mu m$). The parameterisation describes the dry particle flux as a function of the sea water temperature T (in K) and the size-dependent (particle size class k) coefficients a and b.

$$\frac{dF_0}{d \log D_d} = W(U_1 0) \cdot (A_k T_w + B_k) \tag{8.16}$$

$$A_k = a_0 + a_1 D_d + a_2 D_d^2 + a_3 D_d^3 + a_4 D_d^4$$
$$B_k = b_0 + b_1 D_d + b_2 D_d^2 + b_3 D_d^3 + b_4 D_d^4$$

$$\tag{8.17}$$

These coefficients were deduced from fits through experimental data and are given in Table 8.5 and Table 8.6.

8.5.2   *Monahan et al. formulation*

For larger particles (1 ¡ D_p ¡ 10 μm), the Monahan et al. (1986) formulation is used. This formulation is based on laboratory experiments on decaying whitecaps and includes both small droplets resulting from bubble bursting and the coarser spume drops by mechanical disruption of wave crests. The net wet particle flux for particles at 80% RH, with radius r, is given by

$$\frac{dF_0}{Dr_p} = 1.373U_{10}^{3.41}r_p^{-3}(1 + 0057r_p^{1.05}) \times 10^{1.19e^{-B^2}}, B = \frac{0.38 - ^{10}\log(r_p)}{0.65} \tag{8.18}$$

For mass emissions, it was assumed that the particle radius at 80% RH was twice the dry particle radius. This formulation includes an experimental factor describing the decay timescale of a single whitecap.

8.6   Dust sources

The current model includes a dust model with 3 components:

- natural wind blown dust;

- re-suspension by traffic;

- agricultural land management.

Natural dust emission from erodible surfaces is a complex process. It requires several parameterizations and input of e.g. soil characteristics. The parameterizations of agricultural land-management and road re-suspension are described in Schaap et al. (2009) and are only briefly summarized here.

8.6.1   *Natural wind-blown dust*

When the wind blows over a surface, it exacts a certain force on it which may mobilize soil material. The mobilization of a particle is controlled by the gravitational force, inter-particle cohesion, and wind-shear stress acting on the particle, all depending on the particle size. The effect of this mobilization is an increase of the fine and coarse mode concentrations of dust in the atmosphere.

The wind blown dust model in LOTOS-EUROS is based on the work by Marticorena and Bergametti (1995), which describes the saltation of coarse particles, which release smaller particles when hitting the ground (salt blasting). We follow the approach of Mokhtari et al. (2012) with some adaptations.

Input to the dust model is:

- a land use map;

- a soil texture map;

- a potential/preferential sources map;

- soil water content (available from meteorological input data);

- snow cover (available from meteorological input data), no emission when surface covered by snow;

- roughness length;

- wind speed;

The **land use map** is used to determine the areas with bare soil. These are the land use classes 'desert' and 'arable land' (see Chapter 9). Arable land is assumed bare during part of the year, depending on the regional growing seasons. Currently dust emissions from bare agricultural land are switched off since regional differences were not captured satisfactorily with parameter settings that are uniform over the modeling domain.

The **soil texture map** provides a description of the particle sizes present in the soil. LOTOS-EUROS uses the STATSGO map, based on the work by Zobler (1986), as used by RegCM4[3]. This is a high-resolution (2 minutes) global database. The USDS textures in the map can be related to grain size distributions based on mass. It is assumed that soil particles are distributed in size according to logarithmic normal distribution. Parameters for this distribution for the USDA soil texture classes are are presented in Table 8.7.

Table 8.7   USDA soil textures and assigned properties.

	soil particle size distribution								
	mode 1			**mode 2**			**mode 3**		
	f_m	$D_{s,g3,1}$	$\sigma_{g,1}$	f_m	$D_{s,g3,2}$	$\sigma_{g,2}$	f_m	$D_{s,g3,3}$	$\sigma_{g,3}$
texture class	%	μm	1	%	μm	1	%	μm	1
clay	50	100	1.8	0	10	1.8	50	0.5	1.8
silty clay	60	100	1.8	0	10	1.8	40	0.5	1.8
silty clay loam	30	210	1.7	50	50	1.7	20	2.5	1.8
clay loam	20	125	1.7	50	50	1.7	30	1	1.8
silt	45	520	1.6	40	75	1.7	15	2.5	1.8
silt loam	50	520	1.6	35	100	1.7	15	5	1.8
sandy clay	65	100	1.8	0	10	1.8	35	1	1.8
loam	35	520	1.6	50	75	1.7	15	2.5	1.8
sandy clay loam	30	210	1.7	50	75	1.7	20	2.5	1.8
sandy loam	60	520	1.6	30	100	1.7	10	5	1.8
loamy sand	60	690	1.6	30	100	1.7	10	10	1.8
sand	90	1000	1.6	10	100	1.7	0	10	1.8

A **preferential sources map** is used to determine areas that have more potential to emit dust (e.g. dry river or lakes). Such a map basically corrects for impacts of topography on the wind velocity that are beyond the resolution of the meteorological model These areas can be inferred from satellite-detected dust events (best approach, but not globally available) but at present a more simple approximation purely based on topographical information is used, following Ginoux et al. (2001). A static global map was constructed and is available as input. The preferential source fraction F_{ps} is determined from minimum and maximum terrain height in the surrounding 10 degrees longitude and latitude of a grid cell with terrain height h according to

$$F_{ps} = \left(\frac{h_{\max} - h}{h_{\max} - h_{\min}} \right)^5 \tag{8.19}$$

There are three instances of **roughness length** as described in (Menut et al. 2013):

1. z_0 representing the roughness elements for momentum at the resolution of the meteorological model which delivers the wind speed, typically at a resolution of 10 km (synopic scale) This is the z_0 which is used for calculation of stability and deposition in the model and is by default set to $z_0 = 0.013m$. This value is representative for smaller uncovered areas in Europe, like dune areas. For large desert areas we recommend a much smaller value, $z_0 = 8 \cdot 10^{-5}$m, consistent with the mesoscale roughness length.

2. a mesoscale (1-10km) roughness length z_{0dust_emis} is used for the calculation of dust emissions only. By default a value of $z_{0dust\_emis} = 8 \cdot 10^{-4}$m is used. For large desert areas we recommend a smaller value, $z_{0dust\_emis} = 8 \cdot 10^{-5}$m.

3. a smooth roughness length z_{0s} representing the local scale (1-100m), related to the soil particle diameter. We use a fixed value $z_{0s} = 3 \cdot 10^{-5}$m, following Mokhtari et al. (2012).

---

[3] http://users.ictp.it/~pubregcm/RegCM4/globedat.htm

The process of sandblasting is an interplay between wind speed, roughness length and soil properties, with large sensitivity to wind speed and roughness length. Currently, fixed values for roughness lengts are defined, but this could be refined by using maps of roughness length, with separate maps for synoptic scale and mesescale roughness length. Also the use of a more refined land use classification provides a better basis for dust emission calculation (clear separation of bare rock and uncovered sands).

8.6.1.1 *Friction velocity threshold*

Dust particles are only released from the surface if the friction velocity is above a certain threshold. The friction Reynolds number is parametrized as a function of the soil particle diameter following Marticorena and Bergametti (1995, Eq. (5)):

$$B(D_s) = a\, D_s{}^x + b \tag{8.20}$$

where D_s is the soil particle diameter in cm, $a = 1331$ cm^{-x}, $b = 0.38$, and $x = 1.56$. With this Reynolds number, the following parametrization for the friction velocity threshold for a smooth surface is used in Marticorena and Bergametti (1995, Eg. (6-7)):

$$u_{\star st}(D_s) = \begin{cases} 0.129\, K\, \left(\, 1.928\, B(D_s)\, -\, 1\,\right)^{-0.5} & ,\quad B(D_s) < 10 \\ 0.12\, K\, \left(\, 1\, -\, 0.0858\, e^{-0.0617(B(D_s)-10)}\,\right) & ,\quad B(D_s) \geq 10 \end{cases} \tag{8.21}$$

in cm/s, were D_s is the soil particle diameter in cm, and:

$$K = \left(\frac{\rho_s\, g\, D_s}{\rho_a}\right)^{0.5} \left(1 + \frac{0.006}{\rho_s\, g\, D_s{}^{2.5}}\right)^{0.5} \qquad \text{[m/s]} \tag{8.22}$$

with ρ_s the soil particle density of about 2.65 g/cm^3, ρ_a the air density of about 0.00123 g/cm^3, and g the gravity acceleration in cm/s^2.

When roughness elements are present in the terrain, a larger friction velocity is needed to mobilize the soil particles. The effective friction velocity threshold is therefore larger if the meso-scale roughness length (aeolian z_0) exceeds the local scale roughness length (z_{0s}, or smooth z_0). The effective threshold could be parametrized following Marticorena and Bergametti (1995, Eq. 18-21) as:

$$u_{\star t,r}(D_s, z_0, z_{0s}) = \frac{u_{\star st}(D_s)}{f_r(z_0, z_{0s})} \tag{8.23}$$

with:

$$f_r(z_0, z_{0s}) = 1 - \left(\frac{\ln\left(\frac{z_0}{z_{0s}}\right)}{\ln\left(a\left(\frac{X}{z_{0s}}\right)^p\right)}\right) \tag{8.24}$$

where z_0 and z_{0s} are the meso-scale and smooth roughness lengths in cm, $a = 0.35$, $X = 10$ cm, and $p = 0.8$.

If soil water is present, the soil particles stick to each other and are more difficult to mobilize. The friction velocity threshold will therefore increase with the soil moisture. This effect will be smaller if the soil contains clay, since this material will first absorb a part of the soil moisture.

In Fécan et al. (1999, Eq. (14)) a parametrization is provided for the maximum amount of soil water that can be absorbed without effecting dust mobilization given the clay fraction (original formulation is in %):

$$\begin{aligned} w'(c) \;&=\; 3\left(\, 0.0014\,(100\,c)^2 \,+\, 0.17\,(100\,c)\,\right)/100 \qquad \text{[(kg water)/(kg soil)]} \\ &\quad 0.053 < w' < 0.15 \end{aligned} \tag{8.25}$$

where c is the clay mass fraction in (kg clay)/(kg soil), and the result w' the gravimetric soil moisture in mass (kg water)/(kg soil). The factor 3 and mininum and maximum value of w' are taken from Mokhtari et al. (2012).

If soil water is present, a growth factor for the friction velocity threshold could be parametrized using Fécan et al. (1999, Eq. (15)), where the original parametrization is in %:

$$f_w(c, w) = \begin{cases} 1 & , \quad w \leq w'(c) \\ \left[1 + 1.21 \; (\; 100 \; w \; - \; 100 \; w'(c) \;)^{0.68} \right]^{0.5} & , \quad w > w'(c) \end{cases} \tag{8.26}$$

with w and $w'(c)$ the gravimetric soil moisture and threshold in (kg water)/(kg soil).

Including the soil moisture and clay fraction factor, the total friction velocity threshold becomes:

$$u_{\star t}(D_s, z_0, z_{0s}, c, w) \; = \; c_{T1} u_{\star st}(D_s) \, f_t(z_0, z_{0s}, c, w) \tag{8.27}$$

with the total friction velocity threshold factor:

$$f_t(z_0, z_{0s}, c, w) \; = \; \frac{f_w(c, w)}{f_r(z_0, z_{0s})} \tag{8.28}$$

This factor depends on space (grid cell, texture in cell) and time (soil water content). A tuning constant c_{T1} with a value of 0.66 was used to modify the threshold uniformly over the domain, the value is taken from by Heinold et al. (2007).

8.6.1.2 *Horizontal flux*

Following Marticorena and Bergametti (1995, Eq.(28)) the horizontal air flux is proportional to a function of friction velocity and its threshold:

$$F_h(u_\star, u_{\star t}) \; \sim \; \begin{cases} 0 & , \quad u_\star \leq u_{\star t} \\ \frac{\rho_a}{g} \, u_\star^3 \, \left(1 + \frac{u_{\star t}}{u_\star}\right) \left(1 - \left(\frac{u_{\star t}}{u_\star}\right)^2\right) \quad \text{[(kg air)/m/s]} & , \quad u_\star > u_{\star t} \end{cases} \tag{8.29}$$

where ρ_a is the air density in kg/m^3, g the gravitation acceleration in m/s^2, $u_\star$ is the meso-scale friction velocity in m/s, and $u_\star$ the threshold.

After eq. (8.27) we write for $u_\star > u_{\star t}$:

$$F_h(u_\star, D_s, f_t) \; \sim \; \frac{\rho_a}{g} \, u_\star^3 \, \left(1 + \frac{u_{\star st}(D_s) \, f_t}{u_\star}\right) \left(1 - \left(\frac{u_{\star st}(D_s) \, f_t}{u_\star}\right)^2\right) \tag{8.30}$$

8.6.1.3 *Vertical aerosol flux*

The vertical aerosol suspension due to saltation is related to the horizontal air flux:

$$G \; = \; \alpha \, F_h \qquad \text{[(kg aerosol)/m}^2\text{/s]} \tag{8.31}$$

For the sandblasting efficiency α different parametrizations have been proposed. In previous versions of LOTOS-EUROS the parameterization by Alfaro and Gomes (2001) was used, which is now replaced by the approach of Shao (2001) which has a less strong nonlinear sensitivity to soil characterization than other parameterizations found in literature.

$$\alpha(D_s, D_d) \; = \; \frac{2}{3} \, \frac{\rho_s}{\rho_d} \, \frac{\beta(D_s, D_d) \, \gamma \, g}{[u_{\star t}(D_d)]^2} \tag{8.32}$$

with:

$$\gamma \; = \; 2.5 \tag{8.33}$$

$$\beta(D_s, D_d) \; = \; \left[0.125 \times 10^{-4} \, \ln(D_s) \, + \, 0.328 \times 10^{-4}\right] \, e^{-140.7 \, D_d \, + \, 0.37} \tag{8.34}$$

where D_s is the diameter of the soil (saltating) particle in mm, and D_d is the diameter of the suspended dust particle in mm, and only for $\beta > 0$.

8.6.1.4   Total flux

For each texture class, the size distribution of soil particles should be used to compute the total flux. The relative importance of a soil particle diameter is related to area that it covers; therefore, the cross-section should be used as weight for the diameters. As function of soil texture s, friction velocity $u_\star$, threshold factor f_t, and aerosol diameter D_a the total flux becomes:

$$
\begin{aligned}
G(s, u_\star, f_t, D_a) &= \int_{D_s} \alpha(D_s, D_d)\, F_h(u_\star, D_s, f_t)\, \mathrm{d}C \,/\, C_s && \text{(8.35a)} \\
&= \int_{D_s} \alpha(D_s, D_d)\, F_h(u_\star, D_s, f_t)\, \frac{\mathrm{d}C}{\mathrm{d}\ln D}\, \mathrm{d}\ln D_s \,/\, C_s && \text{(8.35b)} \\
&= \sum_{j=1}^{3} m_j \int_{D_s} \alpha(D_s, D_d)\, F_h(u_\star, D_s, f_t) \times && \text{(8.35c)} \\
&\quad\quad \frac{C(D_s)}{\rho_s\, V(D_s)}\, \phi(\ln D_s; \ln D_{s,g3,j}, \ln^2 \sigma_{g,j})\, \mathrm{d}\ln D_s \,/\, C_s && \text{(8.35d)}
\end{aligned}
$$

where normation ensures that relative importance of a soil diameter in the surface area is used:

$$
C_s = \sum_{j=1}^{3} m_j \int_{D_s} \frac{C(D_s)}{\rho_s\, V(D_s)}\, \phi(\ln D_s; \ln D_{s,g3,j}, \ln^2 \sigma_{g,j})\, \mathrm{d}\ln D_s \tag{8.36}
$$

For on-line calculation of dust emissions, evaluation of Eq.(8.35) could become expensive. Therefore, a four-dimensional lookup table with evaluations of G has been created. The entries in the table are:

- the soil texture class s (currently 13);

- friction velocity $u_\star$ between 0.0 and 1.0;

- friction velocity threshold factors f_t between 0.0 and 10.0;

- mass distribution geometric mean diameters for the dust aerosols in the model.

If the actual $u_\star$ or f_t exceeds the maximum then last value is used.

The effective vertical dust flux F_v is given by

$$
F_v = \delta C_T G \tag{8.37}
$$

with δ the fraction of erodible area in the grid cell and C_T a tuning constant. This constant has impact on the total emitted aerosol but not on the number and location of modeled events. Ideally no tuning is necessary and C_T is set to one. Since a wide range of bare areas, varying from European dune landscape to the Sahara, has to be represented by a single set parameter values, C_T is set to 0.5. This is a compromise between modeling the number of events with vertical dust emissions and the emission strength per event.

8.6.2   Re-suspension by traffic

Traffic-generated fugitive dust is a predominant source of atmospheric pollution at roadside locations. The contact of the tires with the road and the turbulence in the air caused by the movement of the car induce the uplift of particles that reside on streets and roads (asphalt, concrete) or from the road itself (dirt roads).

A detailed description of the re-suspension model in LOTOS-EUROS is provided in Schaap et al. (2009, section 5.3). The input to this model is:

- a map of average traffic intensities per vehicle class and road type;

- time factors to describe the actual intensity at each moment;

- an estimate of the amount of dust present on a certain road type; this uses a parameterisation based on the average soil water content in a region;

- an estimate of the contribution of sanding of roads;

- rain and snow fields from the meteorological input.

From this, the parameterisations provide an estimate of the amount of dust aerosol released from the roads present in a grid cell.

8.6.3   *Agricultural land-management*

Soil erosion resulting from land-management activities is another source of dust aerosol. This source only includes the release of dust due to crushing and uplift processes by agricultural vehicles; the description of this process is therefore related to that of resuspension by traffic. For a complete description of the agricultural land-management emissions we refer to Schaap et al. (2009, section 5.4). In summary, the emission is derived from:

- maps of land fractions with arable soils;

- time profiles of expected intensity of land-management activities;

- emission factors relating activities to dust aerosol release;

- rain, snow, and temperature fields from the meteorological input.

Dedicated research on emission factors for aerosols is still preliminary, mainly caused by an insufficient amount of reliable observations. The description of this emission is therefore rather simple in LOTOS-EUROS.

8.7   Forest fire emissions

Emissions from forest fires could lead to extremely high concentrations of trace gasses and aerosols at ground level. A fire emits all kind of burning products, from carbon monoxide to undefined particulate matter. The emission strength of a fire is highly uncertain, since it depends on uncertain parameters such as current vegetation, the reservoir of burnable material at the ground, meteorological conditions, the burning period, etc. The location were fires occur(ed) are usually better known, since fires are usually ob-served from the ground or by satellite.

Due to the irregular distribution of fires in space and time, a dedicated fire inventory should be used to model the emissions. For LOTOS-EUROS two data sets are supported.

8.7.1   *GFAS fire emissions*

Most often used is the GFAS fire product from the CAMS (or former MACC) services project is available (Kaiser et al. 2012, Rémy et al. 2017). The emission of the most important trace gasses from fire events is available as a daily average. Most of the emitted tracers can be assigned directly to the equivalent LOTOS-EUROS tracer; the higher organic components are assigned to the mixture of carbon-bounds that represent their molecular structure. These emissions are defined on a regular grid of $0.1° \times 0.25°$ resolution.

Table 8.8   Mass contribution of several elements to sea salt

Element	Mass contribution (g/g)
Na	0.308
Cl	0.554
Mg	0.038
S	0.026
K	0.011
Ca	0.011

In older versions of LOTOS-EUROS, fire emissions were assigned to the second model layer. Since Version 2.2.002 fire emissions are distributed over the vertical with half of the emissoins divided over the layers covering altidudes between altitude of plume bottom ('apb') and the mean altitude of maximum injection ('mami') , and half of the emissions devided over the layers covering altitudes between mean altitude of maximum injections and altitude of plume top ('apt') with weighing on layer thickness. The layer containing mean altitude of mean injection is counted twice, guaranteeing maximum injection in that layer with a very simple approach. When the mean altitude of maximum injection is above the model top, fire emissions are not taken into account. Altitude of plume bottom is only available since July 2018. When altitude of the plume bottom is not available, the altitude of the plume bottom is estimated to be 300 m lower than 'mami'. When 'mami' is equal to zero, a smouldering fire is assumed and emissions are injected at surface level.

8.7.2   SILAM fire emissions

For research projects also an interface to the SILAM fire emission product (Sofiev et al. 2009) was available. The SILAM fire product (IS4FIRES) has become part of the operational CAMS-GFAS fire data since July 2018 as an additional variable (injection heigth), but is currently not used.

8.8   Heavy metals

Emissions of lead and cadmium are described in section 11.2.

8.9   Base cations

Base cations (Na, Mg, Ca, K) are emitted by a host of anthropogenic sources and are part of the particulate matter emission data. Hence, normally a speciation of PM to separate the base cations is not performed, but dedicated inventories have been constructed in the past. Base cations also have a source in primary marine emissions, crustal material for wind-abrasion, resuspension by traffic, and re-suspension by agricultural-activities. Marine emissions are calculated based on the emission functions described in section 8.5. They are scaled to the sodium emissions using fixed factors based on the mass ratios of the elements in sea salt (Table 8.8). To calculate the base cation emissions from soils, the above mentioned mineral dust emission fluxes are combined with distributions that provide the contribution of base cations to top soils in Europe.

9 Land use

9.1 Land use data

The term land use describes the type of land that covers the surface. It is used to establish deposition velocities and surface roughness. It is also required to determine biogenic emission fluxes, such as isoprene and terpene emissions from forests. Land use and land cover are also important for calculations of NO emissions from soil, wind blown dust and agricultural emissions from ploughing etc.

The default land use data set that is used in the model is based on CORINE/ Smiatek (EEA 2000), with a grid resolution of 0.0167° (1.9 x 1.2 km^2 at 50° North) in longitude and latitude over Europe and 13 land use categories (Table 9.1). Per grid point, the main category is given, although for large parts of Europe more detailed information is available. The CORINE/Smiatek database has been combined with the tree species map for Europe made by Köble, R. and Seufert (2001), who also used CORINE as basis. This database contains 115 tree species, on a grid of 1 x 1 km^2, with percentage of coverage per grid cell. In parts of the LOTOS-EUROS modeling domain, especially Russia, the Köble tree map provides no information. We have coupled the CORINE/Smiatek land use database to the database on tree species (Builtjes et al. 2006). In this procedure the land use database was leading, meaning that tree species were only appointed to forest areas. In case no tree species information was available for a forest area, the three CORINE forest categories are maintained (deciduous, coniferous, mixed). So, the full tree database contains 115 + 3 categories. The combined data-base has a resolution of $0.0166° \times 0.0166°$ which is aggregated to the required resolution during the start-up of a model simulation. Each grid cell in LOTOS-EUROS is characterized by the fraction of several types of land use in that particular grid cell.

For Europe, it is also possible to use more recent CORINE data (2018 is now implemented) on top of the default CORINE/Smiatek data. This would includes more recent/high resolution information where available,while preserving the information needed for the tree-specific biogenic emissions from the CORINE/Smiatek data and including informaton for countries not covered in the more recent CORINE data.

In order to apply the DEPAC module for dry deposition, the CORINE land use data had to be converted. The conversion of these land use classes is not trivial, and it needs further attention. The conversions we made are listed in Table 9.2.

Table 9.1   Land use classes used in the CORINE/Smiatek database

urban areas
agriculture
grassland
deciduous forest
coniferous forest
mixed forest
water
marsh or wetland
sand or bare rocks
tundra
permanent ice
tropical forest
woodland shrub

Table 9.2   Conversion of land use categories from CORINE to DEPAC

DEPAC	CORINE/Smiatek
grass	grassland
arable	0.5*arable land
permanent crops	0.5*arable land
coniferous forest	coniferous forest + 0.5*mixed forest
deciduous forest	deciduous forest + 0.5*mixed forest + tropical forest + woodland + shrub + 0.5*wetlands
water	water + 0.5*wetlands + snow or ice
urban	urban area
short grassy	tundra
desert	sand or bare rocks

For areas outside Europe, the Global Land Cover 2000 map may be used. Also for this land use map a translation to depac classes is made in the model code. This land cover database is not linked to a tree species database and can be used together with MEGAN for biogenic emissions.

Land cover data are static data, whereas snow cover may effect vertical stability and deposition efficiencies. This is accounted for in the roughness length, deposition and vertical mixing pararameterizations.

9.2   Land-sea mask

A land-sea mask is needed in order to separate inland water from large bodies of salty water (for the land use class water in CORINE). It is used for two purposes:

1. identification of areas from which sea salt aerosol is generated.

2. Formulation of roughness length depending on wave height (wind speed).

The land-sea mask is based on a GIS map[1]. The polygon map was gridded to the GLC grid at 1/112 degrees resolution. A few modifications were made: Black sea, Caspian sea and sea of Azov where put to "ocean or sea" instead of "perennial inland water" since they are so large that waves may develop that have significant impact on deposition velocity. When a land-sea mask is made for other areas in the world, also manual modifications may be necessary for optimal performance. For inland water a fixed roughness length is used, which is generally lower than the wind-speed dependent roughness length of large open water bodies.

A dependency of the sea surface roughness on the wave height is included. Over grid cells with more than 90% water, the wave height is calculated as function of ten meter wind speed U_{10} in m/s:

$$h_{\text{wave}} = 0.0617 U_{10}^{1.52} \tag{9.1}$$

This function is a fit, applicable for open water conditions. The associated surface roughness z_0 $[m]$ is calculated as

$$z_0 = h_{\text{wave}}/30. \tag{9.2}$$

---

[1] *"World Water Bodies"*, version 2011, last updated 10-2-2015. Created by *Delorme Publishing* and distributed by ESRI, http://library.duke.edu/data/files/esri/esridm/2013/world/data/hydropolys.html

10   Boundary and initial conditions

10.1   Overview

Boundary conditions are concentrations outside the model domain that are necessary to simulate concentrations inside the domain. The LOTOS-EUROS model requires horizontal boundary conditions for the Western, Eastern, Southern and Northern edges of the domain, and vertical boundary conditions for the atmosphere above the model top. The concentrations taken as boundary conditions are preferably taken from simulations done with an external model that runs on a larger domain (probably global). After interpolation in space and time, these concentrations are transported into the domain by advection and/or vertical mixing.

Table 10.1 shows an overview of the supported boundary conditions, the dimension of the concentrations (2D (x,y), 3D (x,y,z) or 4D (x,y,z,t)), the components, and when these conditions are used. A detailed description is provided in the remainder of this chapter.

Table 10.1   Overview of supported boundary conditions

source	dimensions	components	when used
climatologies	2D constant	various	default
CAMS (MACC)	4D	reactive gasses and aerosols	common
EMEP	3D monthly	CBM, aerosols	optional
TM5	4D or 3D monthly	CBM, aerosols	optional
LOTOS-EUROS	4D	all	zooming

The order in which these sources are included as boundary conditions determines which values are actually used for transport into the model. If two sources provide concentrations for the same tracer, the latter source replaces the previous ones. The source with the highest spatial or temporal detail should therefore be included as the last one.

Most boundary conditions are currently taken from output of the CAMS services.

10.2   Climatologies

Various climatological data are in use to fill boundary conditions with reasonable values. All of these climatologies are constant in time, and spatially rather coarse or depend only on latitude and height. Such climatological concentration fields do not supply detailed information , and are therefore preferably replaced by more detailed fields from 4D models. However, for some of the model tracers the climatologies are the only source: mainly the carbon-bond tracers that are specific to the chemistry scheme and those for non-standard tracers such as heavy-metals (see section 11.3) and POPs.

10.3   CAMS global products

CAMS (www.gmes-atmosphere.eu) is a European Union funded service to provide forecasts and re-analyses of trace gasses and aerosols at global and/or European scale. The global services of CAMS provide daily simulations of reactive gasses and aerosols at global scale which are currently the most common source of boundary conditions for LOTOS-EUROS.

From October 2014 onwards, the global simulations are computed with the C-IFS model, a special version of ECMWF's IFS model including aerosols and trace gasses (Flemming et al. 2015). Before the introduction of C-IFS, a similar service was provided under the umbrella of the MACC projects or the initial GEMS project: MACC/R-AER provided aerosol simulations using an extended IFS model, and MACC/G-RG provided reactive gasses using the MOZART model coupled to IFS (Flemming et al. 2009).

Various data sets from CAMS, MACC, or GEMS are available, with each their content, resolution, and format depending on the originating model and post processing. These data sets are therefore rather heterogeneous; the longest uniform series a re-analysis from 2003-2012 with a coupled IFS-MOZART system.

For how to enable these data sets we refer to the User Guide.

10.4   EMEP climatologies

Monthly boundary conditions from the EMEP model are available for use as boundary conditions. Advantage of these boundary conditions is that they were produced with a single model, and are therefore not subject to changes in model version as seen in the CAMS/MACC products.

10.5   TM5 simulations

The TM5 model Huijnen et al. 2010 is a global 3D atmospheric chemistry-transport model. It allows the definition of arbitrary zoom regions, which are 2-way nested into the global model. Thus simulations at relatively high spatial resolution (currently $1° \times 1°$ longitude-latitude) can be performed over selected regions with boundary conditions always, for consistency, provided by the global model. The definition of vertical layers is linked to the vertical layers of the ECMWF model. The version of TM5 that focuses on the troposphere uses a chemistry scheme similar to LOTOS-EUROS.

Two types of TM5 simulations are available as boundary conditions for LOTOS-EUROS. At high temporal resolution (3 or 6 hourly), the model provides simulations of the most common trace gases (ozone, nitrogen oxides, carbon monoxide, etc). In addition, monthly averaged concentration fields are available for the less common tracers (carbon-bonds, radicals, etc.).

10.6   LOTOS-EUROS simulations

For a model simulation on a small domain and at higher resolution, a so-called zoom-run, the boundary conditions can be filled with concentrations simulated with output data available from model runs over a larger domain and lower resolution. To be suitable for application as a boundary condition such model output should include saved 3D concentration fields for the most important species at hourly resolution. Being provided as such, these input data can be treated in a similar way as boundary condition input taken from, for example, the output of a global model to feed the zoom-run. Boundary conditions from the input model run should be the last source of boundary condition values applied, since it is likely that these are in best agreement with the setup of the zoom-run. Note that when applied in this way, it is not necessary that all species were given as output: for the species not included in the boundary condition model run, the previous applied data source is retained.From v2.2.003 onwards, the default is to output all advected tracers as input for a zoom run, to guaruantee a uniform approach. In older versions the vertical layers of the boundary simulation had to be identical to the layers of the nested simulation. We refer to the user guide for technnical details.

10.7   Initial conditions from boundary conditions

For several tracers, boundary conditions are available. These boundary conditions can be used to initialize the model at the first time step. Initial boundary conditions are usually taken from the output of an external (global) model that provides 3D concentrations fields at regular spatial and temporal resolution. After the appropriate interpolation, both in space and time these can serve as initial conditions. If for some tracers the boundary conditions are only defined on the edges of the model domain, the values are interpolated between the western and eastern edges of the domain. The order in which initial conditions are assigned is the same as is used to assign the boundaries themselves. Data sets with largest spatial detail are included last, in order to replace concentrations from less detailed initial (and boundary) condition input data sets.

10.8   Initialization from previous run

Model concentrations can also be initialized from a preceding LOTOS-EUROS model run. To do this, the preceding model run should provide a restart file. This restart file contains all data necessary to continue a model run without the need of a spin-up time period; this includes 3-D concentration fields at start time, but also concentration fields and other fields (e.g. meteorology) from the previous time step. Currently the restart file contains the following entities:

- concentrations of all tracers;

- aerosol water content;

- cell volumes (preceding values are needed for the first adjustment of layer heights);

- atmospheric stability class (preceding values are used to limit the change from one time step to the other);

- average NH3 concentrations of preceding month (used for the compensation point ammonia; see chapter on dry deposition).

If during a first model run a restart file has been saved and a second run is started at the time were the first run has ended and initialized from the re-start file, model results are exactly the same as what would have been achieved with a single long model run.

11 Heavy metals

11.1 Introduction

LOTOS-EUROS focuses on the heavy metals cadmium (Cd) and lead (Pb). After emission these are transported and deposited as aerosols.

11.2 Emissions

Large sources for heavy metals are the non-ferro industry and combustion processes. Many of the sources are very specific for one metal. Emissions from these metals are taken from a specific TNO emission inventory [Denier van der Gon et al., 2005] but this inventory becomes outdated. Besides anthropogenic sources, heavy metals are also emitted from several natural sources (e.g. volcanoes, forest fires and wind blown dust). Furthermore anthropogenic pollutants can be re-emitted after being deposited at the Earth's surface. The resuspension emissions are included in the model as natural emissions. The natural emissions are chosen in accordance with the natural emissions in the EMEP/MSCE-HM model (Travnikov and Ilyin 2005). In this model the natural lead and cadmium emission fluxes are uniformly distributed over sea and land surfaces and are parameterized as to fit the measured back-ground concentrations. In the LOTOS-EUROS model we use the exact same values, i.e. 160 g lead/ km^2/year and 8 g cadmium/km^2/year from sea surfaces and 220 g lead/km^2/year and 12 g cadmium/km^2/year from soils. In the presence of snow cover the emissions are set to zero. It is assumed that 90% of all naturally emitted lead and cadmium is in the coarse mode and 10% in the fine mode.

11.3 Boundary conditions

For both lead and cadmium we use prescribed boundary conditions at the north, south, west, east and top of our model domain. The values are chosen in agreement with the prescribed boundary conditions used in the regional EMEP/MSCE-HM model (Travnikov and Ilyin 2005), which in turn are based on measurement data. Lowest values are found in Northern Europe and over the Atlantic. High values are found over industrial regions. Table 11.1 presents the prescribed lead and cadmium boundary conditions used within LOTOS-EUROS, from which 90% is in the coarse mode and 10% in the fine mode. Due to their relatively short residence time, the boundary conditions for lead and cadmium will not have a large influence on the concentrations in the center of the model domain. However, the boundary conditions can have influence concentrations close to the boundaries.

Table 11.1 Prescribed boundary conditions for lead and cadmium.

	Lead (ng/m^3)	Cadmium (ng/m^3)
North	0.6	0.02
South	1.5	0.04
West	1	0.03
East	2	0.05
Top	0.1	0.003

Bibliography

Agterberg, R and J Wieringa (1989). *Mesoscale terrain roughness mapping of The Netherlands*. Tech. rep. De Bilt, The Netherlands: KNMI. URL: http://www.sciamachy-validation.org/bibliotheek/knmipubTR/TR115.pdf.

Alfaro, Stéphane C. and Laurent Gomes (Aug. 2001). "Modeling mineral aerosol production by wind erosion: Emission intensities and aerosol size distributions in source areas". *Journal of Geophysical Research: Atmospheres* 106.D16, pp. 18075–18084. DOI: 10.1029/2000JD900339.

Banzhaf, S., M. Schaap, A. Kerschbaumer, E. Reimer, R. Stern, E. van der Swaluw, and P. Builtjes (2012). "Implementation and evaluation of pH-dependent cloud chemistry and wet deposition in the chemical transport model REM-Calgrid". *Atmospheric Environment* 49, pp. 378–390. DOI: 10.1016/j.atmosenv.2011.10.069.

Beck, Hylke E., Niklaus E. Zimmermann, Tim R. McVicar, Noemi Vergopolan, Alexis Berg, and Eric F. Wood (2018). "Present and future Köppen-Geiger climate classification maps at 1-km resolution". *Nature* 5.D1, p. 180214. DOI: 10.1038/sdata.2018.214.

Briggs, G.A (1971). "Some recent analysis of plume rise observations." In: *S Proc. 2nc Intern. Clean Air Congesss, H.M. Englund and W.T. Berry (Eds).* New York: Academic Press.

– (1975). *Plume rise predictions. In: Lectures on Air Pollution and Environmental Impact Analysis*. American. Meteorological Society, Boston MA.

Brouwer, F. (2005). *Sensitivity of ozone concentrations in the LOTOS-EUROS model*. Tech. rep. Bilthoven, The Nehterlands: RIVM, RIVM report 500045 003.

Builtjes P. Van den Hout, C. and S.D. Reynolds (1982). "Evaluation of the performance of a photochemical dispersion models in practical applications." In: *Proceedings of the 13th ITM*. Ile der Embiez, France: Elsevier.

Builtjes P, D., C. Van de Hout, H. Veldt, J. Huldy, W. Hulshoff, Basting, and R. van Aalst (1980). "Application of a photochemical dispersion model tot he Netherlands and its surroundings". In: *Proceedings of the 11th ITM*. Amsterdam, The Netherlands: Elsevier.

Builtjes, P.J.H. (1992). *The LOTOS-Long Term Ozone Simulation-project, Summary report*. Tech. rep. TNO, TNO ReportR 92/240.

Builtjes, P.J.H., A. Bleeker, H.A.C. Denier van der Gon, M. Schaap, and A. Visschedijk (2006). *Summary of the contribution of TNO to the UBA-project FKZ 202 43270*. Tech. rep. Apeldoorn, The Netherlands, TNO report 2007-A–R0241.

Businger, J. A., J. C. Wyngaard, Y. Izumi, and E. F. Bradley (Mar. 1971). "Flux-Profile Relationships in the Atmospheric Surface Layer". *Journal of the Atmospheric Sciences* 28.2, pp. 181–189. DOI: 10.1175/1520-0469(1971)028<0181:FPRITA>2.0.CO;2.

Carter, W.P.L (1994). *Calculation of reactivity scales using an updated Carbon Bond IV mechanism*. Tech. rep. San Rafael, CA 94903, USA: Systems Applications International (SAI).

Denier van der Gon, H.A.C., A. Visschedijk, H. van der Brugh, and R. Dröge (2010). *A high resolution European emission data base for the year 2005. A contribution to the UBA-Project PAREST: Particle Reduction Strategies*. Tech. rep. Utrecht, The Netherlands: TNO, TNO report TNO-034-UT-2010-01895_RPT-ML.

Dentener, Frank J. and Paul J. Crutzen (1993). "Reaction of N 2 O 5 on tropospheric aerosols: Impact on the global distributions of NO x , O 3 and OH". *Journal of Geophysical Research* 98.D4, p. 7149. DOI: 10.1029/92JD02979.

Donahue, N. M., A. L. Robinson, and S. N. Pandis (2009). "Atmospheric Organic Particulate Matter: From Smoke to Secondary Organic Aerosol". *Atmos. Environ* 43, 94–'06. DOI: 10.1016/j.atmosenv.2008.09.055.

Donahue, N. M., A. L. Robinson, C. O. Stanier, and S. N. Pandis (2006). "Coupled partitioning, dilution and chemical aging of semivolatile organics". *Environ. Sci. Technol.,* 40.8, pp. 635–2643.

ECMWF (Sept. 2021). "IFS Documentation CY47R3 - Part IV Physical processes". In: 4. ECMWF. DOI: 10.21957/eyrpir4vj.

EEA (2000). *CORINE Land Cover 2000.* URL: dataservice.eea.eu.int.

Egmond, N.D. and H. van Kesseboom (1981). *Numerieke verspreidingsmodellen voor de interpretatie van de meetresultaten van het nationaal meetnet voor luchtverontreininging.* Tech. rep. Bilthoven: RIVM, RIVM Report 227905048.

ENVIRON (2010). *CAMx User Guide, Comprehensive air quality model with extensions, Version 5.20.* Tech. rep. ENVIRON International Corporatoin, 279pp.

EPA (1999). *Science algoritms of the EPA models-3 community multiscale air quality (CMAQ) modeling system.* Tech. rep. EPA/600/R-99/030.

Erisman, J.W and M Schaap (May 2004). "The need for ammonia abatement with respect to secondary PM reductions in Europe". *Environmental Pollution* 129.1, pp. 159–163. DOI: 10.1016/j.envpol.2003.08.042.

Farina, S.C. and S.N Adams P.J.and Pandis (2010). "Modeling global secondary organic aerosol formation and processing with the volatility basis set: Implications for anthropogenic secondary organic aerosol". *Journal of Geophysical Research D: Atmospheres* 115.9.

Fécan, F., B. Marticorena, and G. Bergametti (Jan. 1999). "Parametrization of the increase of the aeolian erosion threshold wind friction velocity due to soil moisture for arid and semi-arid areas". *Annales Geophysicae* 17.1, pp. 149–157. DOI: 10.1007/s00585-999-0149-7.

Fehsenfeld, Fred, Jack Calvert, Ray Fall, Paul Goldan, Alex B. Guenther, C. Nicholas Hewitt, Brian Lamb, Shaw Liu, Michael Trainer, Hal Westberg, and Pat Zimmerman (Dec. 1992). "Emissions of volatile organic compounds from vegetation and the implications for atmospheric chemistry". *Global Biogeochemical Cycles* 6.4, pp. 389–430. DOI: 10.1029/92GB02125.

Flemming, J., V. Huijnen, J. Arteta, P. Bechtold, A. Beljaars, A.-M. Blechschmidt, M. Diamantakis, R. J. Engelen, A. Gaudel, A. Inness, L. Jones, B. Josse, E. Katragkou, V. Marecal, V.-H. Peuch, A. Richter, M. G. Schultz, O. Stein, and A. Tsikerdekis (Apr. 2015). "Tropospheric chemistry in the Integrated Forecasting System of ECMWF". *Geoscientific Model Development* 8.4, pp. 975–1003. DOI: 10.5194/gmd-8-975-2015.

Flemming, J., A. Inness, H. Flentje, V. Huijnen, P. Moinat, M. G. Schultz, and O. Stein (Dec. 2009). "Coupling global chemistry transport models to ECMWF's integrated forecast system". *Geoscientific Model Development* 2.2, pp. 253–265. DOI: 10.5194/gmd-2-253-2009.

Fountoukis, C. and A. Nenes (Sept. 2007). "ISORROPIA II: a computationally efficient thermodynamic equilibrium model for K+-Ca2+-Mg2+-NH4+-Na+- SO42–NO3–Cl–H2O aerosols". *Atmospheric Chemistry and Physics* 7.17, pp. 4639–4659. DOI: 10.5194/acp-7-4639-2007.

Gery, Michael W., Gary Z. Whitten, James P. Killus, and Marcia C. Dodge (1989). "A photochemical kinetics mechanism for urban and regional scale computer modeling". *Journal of Geophysical Research* 94.D10, p. 12925. DOI: 10.1029/JD094iD10p12925.

Ginoux, P., M. Chin, I. Tegen, B. Prospero J.M.and Holben, O. Dubovik, and S.-J. Lin (2001). "Sources and distributions of dust aerosols simulated with the GOCART model". *Journal of Geophysical Research D: Atmospheres*. DOI: 10.1029/2000JD000053.

Giorgi, Filippo (1988). "Dry deposition velocities of atmospheric aerosols as inferred by applying a particle dry deposition parameterization to a general circulation model". *Tellus B* 40B.1, pp. 23–41. DOI: 10.1111/j.1600-0889.1988.tb00210.x. eprint: https://onlinelibrary.wiley.com/doi/pdf/10.1111/j.1600-0889.1988.tb00210.x.

Guenther, A., T. Karl, C. Harley P.and Wiedinmyer, P.I. Palmer, and C. Geron (2006). "Estimates of global terrestrial isoprene emissions using MEGAN (Model of Emissions of Gases and Aerosols from Nature)". *Atmospheric Chemistry and Physics* 6, pp. 3181–3210.

Guenther, Alex B., Russell K. Monson, and Ray Fall (1991). "Isoprene and monoterpene emission rate variability: Observations with eucalyptus and emission rate algorithm development". *Journal of Geophysical Research* 96.D6, p. 10799. DOI: 10.1029/91JD00960.

Guenther, Alex B., Patrick R. Zimmerman, Peter C. Harley, Russell K. Monson, and Ray Fall (1993). "Isoprene and monoterpene emission rate variability: Model evaluations and sensitivity analyses". *Journal of Geophysical Research* 98.D7, p. 12609. DOI: 10.1029/93JD00527.

Hammingh, P., H. Thè, F de Leeuw, F. Sauter, A. van Pul, and J. Matthijsen (2001). "A Comparison of 3 Simplified Chemical Mechanisms for Tropospheric Ozone Modeling." In: *Proceedings of EUROTRAC Symposium*. Ed. by J. Midgley, P.M.;. Reuther M.J.; Williams. Garmisch-Partenkirchen, Germany: Proceedings of EUROTRAC Symposium.

Hass, H., P.J.H. Builtjes, D. Simpson, and R. Sternii (Oct. 1997). "Comparison of model results obtained with several european regional air quality models". *Atmospheric Environment* 31.19, pp. 3259–3279. DOI: 10.1016/S1352-2310(97)00066-6.

Heinold, B.I., Helmert J., Hellmuth O., Wolke R., Ansmann A., Marticorena B, Laurent B., and Tegen (2007). "Regional modeling of Saharan dust events using LM-MUSCAT: Model description and case studies". *Journal of Geophysical Research D: Atmospheres*. DOI: 10.1029/2006JD007443.

Hooghiemstra, P.B. (Dec. 2006). *Towards Advection on a Full Reduced Grid for TM5*. Tech. rep. KNMI. URL: https://cdn.knmi.nl/system/data_center_publications/files/000/067/398/original/tr294_hooghiemstra_2006.pdf?1495620749.

Huijnen, V., J. Williams, M. van Weele, T. van Noije, M. Krol, F. Dentener, A. Segers, S. Houweling, W. Peters, J. de Laat, F. Boersma, P. Bergamaschi, P. van Velthoven, P. Le Sager, H. Eskes, F. Alkemade, R. Scheele, P. Nédélec, and H.-W. Pätz (Oct. 2010). "The global chemistry transport model TM5: description and evaluation of the tropospheric chemistry version 3.0". *Geoscientific Model Development* 3.2, pp. 445–473. DOI: 10.5194/gmd-3-445-2010.

Jacob, D (2000). "Heterogeneous chemistry and tropospheric ozone". *Atmospheric Environment* 34.12-14, pp. 2131–2159. DOI: 10.1016/S1352-2310(99)00462-8.

Jacobs, C.M.J. and W.A.J. Van Pul (1996). *Long-range atmospheric transport of persistant Organic Pollutants, I: Description of surface-atmosphere exchange modules and implementation in EUROS.* Tech. rep. Bilthoven: National Institute of Public Health and Environmental Protection (RIVM), Report 722401013. URL: http://www.scopus.com/inward/record.url?eid=2-s2.0-0042351135%7B%5C%7DpartnerID=tZOtx3y1.

Kaiser, J. W., A. Heil, M. O. Andreae, A. Benedetti, N. Chubarova, L. Jones, J.-J. Morcrette, M. Razinger, M. G. Schultz, M. Suttie, and G. R. van der Werf (Jan. 2012). "Biomass burning emissions estimated with a global fire assimilation system based on observed fire radiative power". *Biogeosciences* 9.1, pp. 527–554. DOI: 10.5194/bg-9-527-2012.

Kasibhatla, P., W. L. Chameides, B. Duncan, M. Houyoux, C. Jang, R. Mathur, T. Odman, and A. Xiu (Dec. 1997). "Impact of inert organic nitrate formation on ground-level ozone in a regional air quality model using the Carbon Bond Mechanism 4". *Geophysical Research Letters* 24.24, pp. 3205–3208. DOI: 10.1029/97GL03260.

Köble, R. and Seufert, G. (2001). "Novel Maps for Forest Tree Species in Europe." In: *Proceedings of the conference 'A changing atmosphere'*. Torino, Italy, September 17–20 2001.

Kuenen, J. J. P., S. Dellaert, Visschedijk, Jalkanen J.-P., I. Super, and H. A. C. Denier van der Gon (Jan. 2022). "CAMS-REG-v4: a state-of-the-art high-resolution European emission inventory for air quality modelling". *Earth Syst. Sci. Data* 14.14, pp. 491–414. DOI: 10.5194/essd-14-491-2022.

Kuenen, J. J. P., A. J. H. Visschedijk, M. Jozwicka, and H. A. C. Denier van der Gon (Oct. 2014). "TNO-MACC_II emission inventory; a multi-year (2003-2009) consistent high-resolution European emission inventory for air quality modelling". *Atmospheric Chemistry and Physics* 14.20, pp. 10963–10976. DOI: 10.5194/acp-14-10963-2014.

Lane, T.E., N.M. Donahue, and S.N. Pandis (2008). "Simulating secondary organic aerosol formation using the volatility basis-set approach in a chemical transport model". *Atmospheric Environment* 42.32, pp. 7439–7451.

Leer, B. van (1977). "Towards the ultimate conservative difference scheme. IV. A new approach to numerical convection". *Journal of Computational Physics* 23.3, pp. 276–299. DOI: https://doi.org/10.1016/0021-9991(77)90095-X.

Leeuw, Frank A A M de and H Jetske van Rheineck Leyssius (1990). "Modeling study of SO x and NO x transport during the January 1985 SMOG episode". *Water, Air and Soil Pollution* 51.3, pp. 357–371. DOI: 10.1007/BF00158232.

Lerdau, M. and M. Keller (May 1997). "Controls on isoprene emission from trees in a subtropical dry forest". *Plant, Cell and Environment* 20.5, pp. 569–578. DOI: 10.1111/j.1365-3040.1997.00075.x.

Lerdau, M.T. (1991). "Plant function and biogenic terpene emission". In: *Trace gas emissions by plants*. Ed. by T.D. Sharkey, E.A Holland, and H.A. Mooney. San Diego Academic Press.

Loon, M. van (1994). *Numerical smog prediction, I: The physical and chemical model.* Tech. rep. Amsterdam, The Netherlands: CWI research report, NM-R9411, ISSN 0169-0388, URL: http://www.cwi.nl/static/publications/reports/NM-1994.html.

– (1995). *Numerical smog prediction II: grid refinement and its application to the Dutch smog prediction model*. Tech. rep. Amsterdam, The Netherlands: CWI, research report, NM-R9523, ISSN 0169-0388. URL: http://www.cwi.nl/static/publications/reports/NM-1995.html.

Manders, A.M.M., M. Schaap, X. Querol, M.F.M.A. Albert, J. Vercauteren, T.A.J. Kuhlbusch, and Hoogerbrugge R. (2010). "Sea salt concentrations across the European continent". *Atmospheric Environment* 44.20. DOI: 10.1016/j.atmosenv.2010.03.028.

Mårtensson, E. M., E. D. Nilsson, G. de Leeuw, L. H. Cohen, and H.-C. Hansson (May 2003). "Laboratory simulations and parameterization of the primary marine aerosol production". *Journal of Geophysical Research: Atmospheres* 108.D9, n/a–n/a. DOI: 10.1029/2002JD002263.

Marticorena, B. and G. Bergametti (1995). "Modeling the atmospheric dust cycle: 1. Design of a soil-derived dust emission scheme". *Journal of Geophysical Research* 100.D8, p. 16415. DOI: 10.1029/95JD00690.

Matthijsen, J., L. L. Delobbe, Sauter F., and L. de Waal (2001). "Changes of Surface Ozone over Europe upon the Gothenburg Protocol Abatement of 1990 Reference Emissions." In: *Proceedings of EUROTRAC Symposium, 2000.* Ed. by P.M Midgley, M.J. Reuther, and M. Williams. Garmisch-Partenkirchen, Germany.

Matthijsen, J., F.J. Sauter, and E.S. de Waal (2002). "Modelling of particulate matter on a European scale." In: *Proceedings of GLOREAM Symposium, 2001*. Ed. by J. Keller and S. Andreani-Aksojoglu. Wengen, Switzerland. URL: http://www.scopus.com/inward/record.url?eid=2-s2.0-39349103202%7B%5C&%7DpartnerID=tZOtx3y1.

McNaughton, K G and B J J M Van Den Hurk (1995). "A 'Lagrangian' revision of the resistors in the two-layer model for calculating the energy budget of a plant canopy". *Boundary-Layer Meteorology* 74.3, pp. 261–288. DOI: 10.1007/BF00712121.

Mentel, Thomas F., Martin Sohn, and Andreas Wahner (1999). "Nitrate effect in the heterogeneous hydrolysis of dinitrogen pentoxide on aqueous aerosols". *Phys. Chem. Chem. Phys.* 1.24, pp. 5451–5457. DOI: 10.1039/A905338G.

Menut, Laurent, Carlos Pérez, Karsten Haustein, Bertrand Bessagnet, Catherine Prigent, and Stéphane Alfaro (June 2013). "Impact of surface roughness and soil texture on mineral dust emission fluxes modeling". *Journal of Geophysical Research: Atmospheres* 118.12, pp. 6505–6520. DOI: 10.1002/jgrd.50313.

Metzger, Swen (2002). "Gas/aerosol partitioning: 1. A computationally efficient model". *Journal of Geophysical Research* 107.D16, p. 4312. DOI: 10.1029/2001JD001102.

Mills, Gina, Harry Harmens, Felicity Hayes, Håkan Pleijel, Patrick Büker, Ignacio González, Rocío Alonso, Jürgen Bender, Elke Bergmann, Victoria Bermejo, Sabine Braun, Helena Danielsson, Giacomo Gerosa, Ludger Grünhage, Per Karlsson, Riccardo Marzuoli, Marcus Schaub, and David Simpson (Apr. 2017). "Mapping critical levels for vegetation". In: LRTAP Conventions. Chap. Revised Chapter 3 of the Manual on Methodologies and Criteria for Modelling and Mapping Critical Loads and Levels and Air Pollution Effects, Risks and Trends.

Mokhtari, M., L. Gomes, P. Tulet, and T. Rezoug (May 2012). "Importance of the surface size distribution of erodible material: an improvement on the Dust Entrainment And Deposition (DEAD) Model". *Geoscientific Model Development* 5.3, pp. 581–598. DOI: 10.5194/gmd-5-581-2012.

Monahan, E.C. and I. O'Muircheartaigh (1980). "Optimal power-law description of oceanic whitecap coverage dependence on wind speed". *Journal of Physical Oceanography* 10, pp. 2094–2099.

Monahan, E.C., D.E. Spiel, and K.L Davidson (1986). "A model of marine aerosol generation via whitecaps and wave disruption". In: *Oceanic Whitecaps and their role in in air/sea exchange*. Ed. by G. Monahan E.C.and Mac Niocaill. Reidel, Norwell, Mass., USA, pp. 167–174.

Nenes, Athanasios, Spyros N. Pandis, and Christodoulos Pilinis (May 1999). "Continued development and testing of a new thermodynamic aerosol module for urban and regional air quality models". *Atmospheric Environment* 33.10, pp. 1553–1560. DOI: 10.1016/S1352-2310(98)00352-5.

Novak, J.H. and T.E. Pierce (1993). "Natural emissions of oxidant precursors". *Water, Air and Soil Pollution* 67, pp. 57–77. DOI: 10.1007/BF00480814.

Poppe, D., Y. Andersson-Sköld, A. Baart, P.J.H. Builtjes, M. Das, F. Fiedler, O Hov, F. Kirchner, M. Kuhn, J.B. Makar P.A.and Milford, M.G.M. Roemer, R. Ruhnke, D. Simpson, W.R. Stockwell, A. Strand, B. Vogel, and H. Vogel (1996). *Gas-phase reactions in atmospheric chemistry and transport models: a model intercomparison.* Tech. rep. Garmisch-Partenkirchen, Germany: Eurotrac report. ISS.

Rémy, S., A. Veira, R. Paugam, M. Sofiev, J. W. Kaiser, F. Marenco, S. P. Burton, A. Benedetti, R. J. Engelen, R. Ferrare, and J. W. Hair (2017). "Two global data sets of daily fire emission injection heights since 2003". *Atmospheric Chemistry and Physics* 17.4, pp. 2921–2942. DOI: 10.5194/acp-17-2921-2017.

Robinson, Allen L., M. Donahue Neil, Manish K. Shrivastava, Emily a Weitkamp, Amy M Sage, Andrew P Grieshop, Timothy E Lane, Jeffrey R Pierce, and Spyros N Pandis (2007). "Rethinking organic aerosols: Semivolatile emissions and photochemical aging". *Science* 315.5816, pp. 1259–1262.

Roemer, M., M. Beekmann, R. Bergström, G. Boersen, H. Feldmann, F. Flatøy, C. Honore, J. Langner, J.E. Jonson, J. Matthijsen, M Memmesheimerm, D. Simpson, P. Smeets, S. Solberg, R. Stern, D. Stevenson, P. Zandveld, and Zlatev Z (2003). "Ozone trends according to ten dispersion models". In: *Eurotrac report, Eurotrac-ISS*. Garmisch-Partenkirchen, Germany.

Schaap, M. (2004). "Anthropogenic black carbon and fine aerosol distribution over Europe". *Journal of Geophysical Research* 109.D18, p. D18207. DOI: 10.1029/2003JD004330.

Schaap, M., M. van Loon, H. M. ten Brink, F. J. Dentener, and P. J. H. Builtjes (June 2004). "Secondary inorganic aerosol simulations for Europe with special attention to nitrate". *Atmospheric Chemistry and Physics* 4.3, pp. 857–874. DOI: 10.5194/acp-4-857-2004.

Schaap, M., A.M.M. Manders, E.C.J. Hendriks, J.M. Cnossen, A.J. Segers, H.A.C. Denier van der Gon, M. Jozwicka, F.J. Sauter, G.J.M. Velders, J. Matthijsen, and P.J.H. Builtjes (2009). *Regional modelling of particulate matter for the Netherlands*. Tech. rep. Netherlands Environmental Assessment Agency (PBL). URL: http://www.rivm.nl/bibliotheek/rapporten/500099008.pdf.

Schaap, M., F. Sauter, G. Boersen, and P. Builtjes (2005). *The integration of LOTOS and EUROS: Activities during 2004.* Tech. rep. Apeldoorn, The Netherlands (in Dutch): TNO-report B&O-A R2005/209,

Scott, B. C. (Sept. 1978). "Parameterization of Sulfate Removal by Precipitation". *Journal of Applied Meteorology* 17.9, pp. 1375–1389. DOI: 10.1175/1520-0450(1978)017<1375:POSRBP>2.0.CO;2.

Seinfeld, John H and Spyros N Pandis (2006). *Atmospheric chemistry and physics : from air pollution to climate change*. Hoboken, N.J. J. Wiley.

Shao, Yaping (Sept. 2001). "A model for mineral dust emission". *Journal of Geophysical Research: Atmospheres* 106.D17, pp. 20239–20254. DOI: 10.1029/2001JD900171.

Shrivastava, M.K., T.E. Lane, N.M. Donahue, S.N. Pandis, and A.L. Robinson (2008). "Effects of gas particle partitioning and aging of primary emissions on urban and regional organic aerosol concentrations". *Journal of Geophysical Research D: Atmospheres* 113.18.

Simpson, D., A. Guenther, C.N. Hewitt, and R. Steinbrecher (1995). "Biogenic emissions in Europe 1. Estimates and uncertainties". *Journal of Geophysical Research D: Atmospheres* 100.D11, pp. 22, 875–22, 890.

Simpson, D, M R Ashmore, L Emberson, and J-P Tuovinen (Apr. 2007). "A comparison of two different approaches for mapping potential ozone damage to vegetation. A model study." *Environmental Pollution* 146.3, pp. 715–25. DOI: 10.1016/j.envpol.2006.04.013.

Slinn, W.G.N. (1982). "Predictions for particle deposition to vegetative canopies". *Atmospheric Environment* 17.7, pp. 1785–1794.

Sofiev, M., R. Vankevich, M. Lotjonen, M. Prank, V. Petukhov, T. Ermakova, J. Koskinen, and J. Kukkonen (2009). "An operational system for the assimilation of the satellite information on wild-land fires for the needs of air quality modelling and forecasting". *Atmos. Chem. Phys.* 9, pp. 6833–6847.

Thunis, P., C. Cuvelier, P. Roberts, L. White, Post, L. Tarrason, S. Tsyro, R. Stern, A. Kerschbaumer, L. Rouil, B. Bessagnet, P. Builtjes, M. Schaap, G. Boersen, and R. Bergstroem (2008). *Evaluation of a Sectoral Approach to Integrated Assessment Modelling including the Mediterranean Sea.* Tech. rep. Eurodelta II report. EUR 23444 EN. DOI: 10.2788/87066..

Tingey, David T, Marybeth Manning, Louis C Grothaus, and Walter F Burns (May 1980). "Influence of Light and Temperature on Monoterpene Emission Rates from Slash Pine". *Plant Physiology* 65.5, pp. 797–801. DOI: 10.1104/pp.65.5.797.

Travnikov, O. and I. Ilyin (2005). *Regional Model MSCE-HM of Heavy Metal Transboundary Air Pollution in Europe.* Tech. rep. EMEP/MSC-E Technical Report 6/2005: Meteorological Synthesizing Centre-East of EMEP.

Tsimpidi, A.P., V.A. Karydis, M. Zavala, W. Lei, L. Molina, I.M. Ulbrich, J.L. Jimenez, and S.N. Pandis (2010). "Evaluation of the volatility basis-set approach for the simulation of organic aerosol formation in the Mexico City metropolitan area". *Atmospheric Chemistry and Physics* 10.2, pp. 525–546.

Turner, D.M., T. CHico, and J.A. Catalano (1986). *Tupos, a multiple source gaussian dispersion algorithm using on-site turbulence data.* Tech. rep. Atmospheric sciences research laboratory, office of research and development, US Environmental protection agency, Research Triangle park, NC.

van Rheineck Leyssius, H J, Frank A A M de Leeuw, and Bert H Kesseboom (1990). "A regional scale model for the calculation of episodic concentrations and depositions of acidifying components". *Water, Air and Soil Pollution* 51.3, pp. 327–344. DOI: 10.1007/BF00158230.

Verwer, J.G., J.G. Blom, M. van Loon, and E.J. Spee (Jan. 1996). "A comparison of stiff ODE solvers for atmospheric chemistry problems". *Atmospheric Environment* 30.1, pp. 49–58. DOI: 10.1016/1352-2310(95)00283-5.

Wesely, M.L. (1989). "Parameterization of surface resistances to gaseous dry deposition in regional-scale numerical models". *Atmospheric Environment* 23.6, pp. 1293–1304. DOI: https://doi.org/10.1016/0004-6981(89)90153-4.

Whitten, G Z, H Hogo, and J P Killus (June 1980). "The carbon-bond mechanism: a condensed kinetic mechanism for photochemical smog." *Environmental science & technology* 14.6, pp. 690–700. DOI: 10.1021/es60166a008.

Wichink Kruit, R.J., M. Schaap, E. Sauter F.J.and Van der Swaluw, and E. Weijers (2012). *Improving the understanding of the secondary inorganic aerosol distribution over the Netherlands.* Tech. rep. Utrecht, The Netherlands: TNO, report TNO-060-UT-2012-00334.

Zanten, M.C. van, F.J. Sauter, R.J. Wichink Kruit, J.A. van Jaarsveld, W.A.J. van Pul, and R.J. Wichink Kruit (2010). *Description of the DEPAC module. Dry deposition modelling with DEPAC_GCN2010.* Tech. rep. Bilthoven, The Nehterlands: Rijksinstituut voor volksgezondheid en Milieu, RIVM report 680180001. URL: https://www.rivm.nl/bibliotheek/rapporten/680180001.pdf.

Zhang, L (2001). "A size-segregated particle dry deposition scheme for an atmospheric aerosol module". *Atmospheric Environment* 35.3, pp. 549–560. DOI: 10.1016/S1352-2310(00)00326-5.

Zobler, L (1986). *A World soil file for global climate modelling.* Technical Memorandum NASA-TM-87802. NASA.

A   Landuse dependent parameters

Table A.1 shows the land use dependent parameters that are used in various parts of the code. They include rougnhess lengts for momentum and heat, roughness length for dust emissions and the roughness length related to canopy top, various coefficients for the dry deposition of particles, coefficients for soil NOx emissions and parameters used in DEPAC for resistances related to vegetation.

Table A.1   Parameters depending on landuse class

	grass	arable land	perm. crops	conif. forest	decid. forest	water	urban	other	desert	ice	savanna	tropical forest	wai	med	sem	wheat	beech	spruce
rougnhess lengths																		
z0_momentum(m)	0.03	0.1	0.25	2	2	0.002	1	0.05	0.013	0.002	0.03		0.002	0.25	0.02	0.1	2	2
z0_heat(m)	0.03	0.1	0.25	2	2	0.002	1	0.05	0.0013	0.002	0.03	2	0.002	0.25	0.02	0.1	2	2
z0_dust (m)									0.0008									
z0_canopytop(m)	0.1	0.33	0.83	6.67	6.67	0.007	3.33	0.17	0.043	0.007	0.1	6.67	0.007	0.83	0.07	0.33	6.67	6.67
z0_h or m snow (m)	0.01														0.01			
Deposition																		
a (-)	1.2	1.2	1.2	1	1	100	1.5	1.2	50	100	1.2	1 100	1.2	50	1.2	1	1	
γ (-)	0.54	0.54	0.54	0.56	0.56	0.5	0.56	0.54	0.58	0.5	0.54	0.56	0.5	0.54	0.54	0.54	0.56	0.54
A (mm)	3	3	2	2	7		10	3			3	7		2		3	7	2
Soil NOx																		
A_bio_no	0.9	0.9	0.9	0.07	0.07	0	0	0	0	0	0.9	0.07	0	0.07	0.9	0.9	0.07	0.07
temp_coeff_no	0.67	0.67	0.67	0.84	0.84	0	0	0	0	0	0.67	0.84	0	0.84	0.67	0.67	0.84	0.84
base_coeff_no	8.8	8.8	8.8	3.6	3.6	0	0	0	0	0	8.8	3.6	0	3.6	8.8	8.8	3.6	3.6
DEPAC																		
rsmin	100	100	100	145	232		100				100	232		100	100	100	232	145
brs	66	66	66	22	25		66				66	25		66	66	66	25	22
be	0	0	0	0	0		0				0	0		0	0	0	0	0
Tmin_bal	5	5	5	-5	10		5				5	10		5	5	5	10	-5
Topt_bal	25	25	25	9	25		25				25	25		25	25	25	25	9
Tmax_bal	45	45	45	35	45		45				45	45		45	45	45	45	35
laimx	6	5	5	5	5		6				5	5		5	6	6	5	5

B   Reactions and rates of the CBM-IV chemical mechanism

In this section we describe the full CBM-IV chemical mechanism of LOTOS-EUROS.

B.1   Species

Table B.1 shows the chemical species used in the CBM-IV implementation.

Table B.1   List of species in the CBM-IV chemistry scheme, as used in LOTOS-EUROS.

| nr.	name	description
1	NO2	Nitrogen dioxide
2	NO	Nitric oxide
3	O3	Ozone
4	ETH	Ethene
5	OLE	Olefin carbon bond (C=C)
6	PAR	Paraffin carbon bond (C-C)
7	ALD	Acetaldehyde
8	FORM	Formaldehyde
9	XYL	Xylene and other polyalkyl aromatics
10	TOL	Toluene and other monoalkyl aromatics
11	CO	Carbon monoxide
12	CH4	Methane
13	SO2	Sulfur dioxide
14	PAN	Peroxyacyl nitrate (based on peroxyacetyl nitrate)
15	MGLY	Methylglyoxal and other aromatic products
16	CRES	Cresol and higher molecular weight phenols
17	HNO2	Nitrous acid
18	HNO3	Nitric acid
19	NH3	ammonia
20	H2O2	Hydrogen peroxide
21	OPEN	Aromatic ring opening product
22	TO2	Toluene-hydroxyl radical adduct
23	ISO	Isoprene
24	ISPD	Isoprene product (lumped methacrolein, methyl vinyl ketone, etc.)
25	NO3	Nitrate radical
26	OH	Hydroxyl radical
27	HO2	Hydroperoxy radical
28	N2O5	Dinitrogen pentoxide
29	C2O3	Acylperoxy radical (based on acetylperoxy)
30	XO2	NO to NO2 conversion from alkylperoxy (RO2) radical
31	XO2N	NO to organic nitrate conversion from alkylperoxy (RO2) radical
32	TERP	terpenes
33	CRO	Methylphenoxy radical

B.2 Photolysis reactions

The clear sky photolysis rate J in min^{-1}, is calculated according to the Roeths flux algorithm (Poppe et al. 1996):

$$J = A \exp\left(B\left[1 - \frac{1}{\cos(C\theta)}\right]\right),$$ (B.1)

with A the photolysis rate at an overhead sun (θ = 0) and C a correction factor to account for the bending of solar radiation through scattering in the atmosphere.

Figure B-1 clear sky reaction rate for the photolysis of NO2 as function of the solar zenith angle
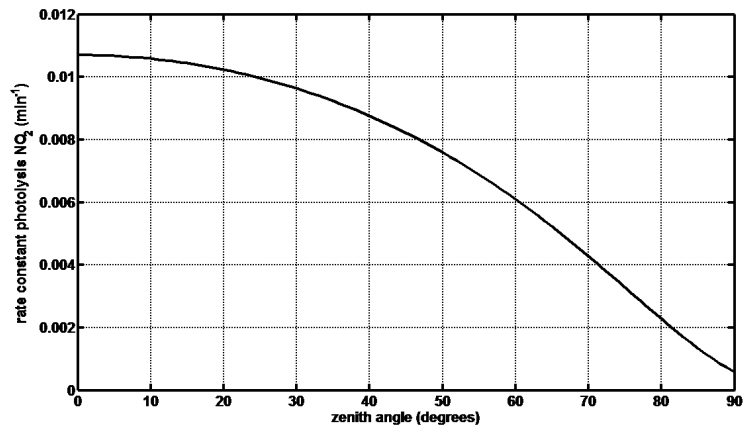
The constants A, B, and C are given in Table B.2. The solar zenith angle θ depends on geographical location, i.e. longitude and latitude, local time of day and is calculated with:

$$\cos(\theta) = ss + cc\cos((t - 12.67)(2\pi/24)).$$

where:

$$
\begin{aligned}
t &= \text{local time of day} \\
D &= 2\pi(\text{julian day } - 1)/365 \\
\Delta &= 0.006918 - 0.399912\cos(D) + 0.070257\sin(D) \\
&\quad -0.006758\cos(2D) + 0.000907\sin(2D) - 0.002697\cos(3D) \\
&\quad +0.00148\sin(3D) \\
ss &= \sin(\theta)\sin(\text{latitude}) \\
cc &= \cos(\theta)\cos(\text{latitude})
\end{aligned}
$$

(B.2)

The photolytic reaction rates are then multiplied by an attenuation factor in case of cloud cover (Fig B-2).

Table B.2   Reactions and clear sky reaction rates for photolytic reactions in the CBM-IV
mechanism, as used in LOTOS-EUROS. Reaction rates (min-1) are calculated according
to Equation B.1

Nr	reaction	A	B	C
1	NO2 + $h\nu \rightarrow$ NO + O3	1.07e-2	1.01319	0.83330
8[a]	O3 + $h\nu \rightarrow$ ftmp$_{O3}$ * $O3$ + ftmp$_{oh}$ * OH	3.22e-5	4.45037	0.78028
16	N2O5 $\rightarrow$ NO3 + NO2	3.79e-5	1.70537	0.80153
	Rk(16) = Rkthermal + Rkphoto			
	Rkthermal = 2.11e16 exp(-10897/T),			
	with T temperature (K)			
19	HNO2 + $h\nu \rightarrow$ OH + NO	8.96e-4	0.99438	0.83295
27	NO3 + $h\nu \rightarrow$ NO2 + O3	2.73e-1	0.29327	0.92401
28	NO3 + $h\nu \rightarrow$ NO	2.74e-2	0.26226	0.92849
33	FORM + $h\nu \rightarrow$ 2*HO2 + CO	4.05e-5	2.06917	0.80267
34	FORM + $h\nu \rightarrow$ CO	4.92e-5	1.60973	0.80184
40	ALD + $h\nu \rightarrow$ CO + FORM + 2*HO2 + XO2	5.4e-6	2.52915	0.79722
47	MGLY + $h\nu \rightarrow$ C2O3 + HO2 + CO	Rk(47) = 0.02 Rk(1)		
74	H2O2 + $h\nu \rightarrow$ 2*OH	7.78e-6	1.91463	0.79810
75	HNO3 + $h\nu \rightarrow$ OH + NO2	5.48e-7	2.86922	0.79561
99	OPEN + $h\nu \rightarrow$ C2O3 + CO + HO2	Rk(99) = 6 Rk(33)		
104	ISPD + $h\nu \rightarrow$ 0.33*CO	Rk(104) = 1.7e-4 Rk(1)		
	+ 0.067*ALD + 0.900*FORM + 0.832*PAR			
	+ 1.03*HO2 + 0.700*XO2 + 1.667*C2O3			

[a] O_3 is transformed into O, but most of it reacts with O_2 to O_3 again. Part of it
reacts with H_2O to form OH. Reaction rates of the lumped reaction depends on
α = ratio between H_2O and O_2 in air: ftmp$_{o3}$=1-α, ftmp$_{oh} = 2\alpha$.
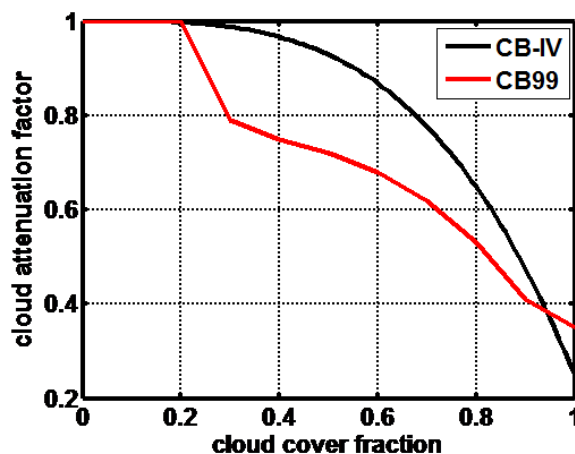

Figure B-2   Cloud attenuation factor as function of cloud cover fraction, as used in the CBM-IV
chemistry scheme (black) and the CB99 scheme (red). To correct for height and zenith
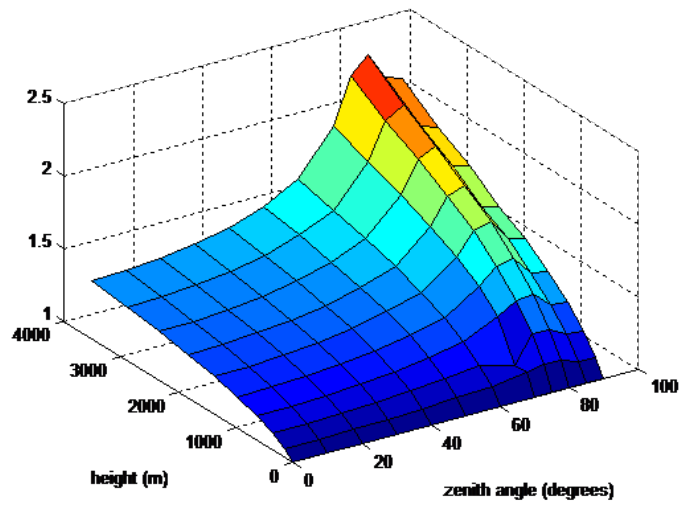angle, an extra correction factor is available; in the current LOTOS-EUROS version it is
not used.

Figure B-3   Correction factor for photolysis rate of NO2, as function of zenith angle and height.

B.3 Non-photolytic reactions

Most other reaction rates are temperature dependent, according to

$$R_k = A \exp(-E/(RT)) \tag{B.3}$$

See for example Fig. B-4.
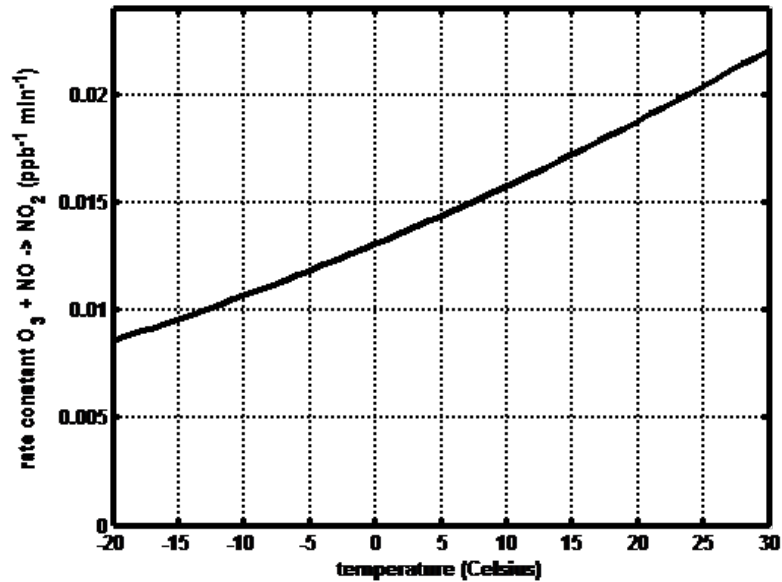
Figure B-4 reaction rate (ppb-2 min-1) of the reaction O3 + NO → NO2.

A Troe-type temperature and pressure dependence is used for the reaction:

C2O3 + NO2 → PAN

by:

$$k_0 = A \left(\frac{T}{T_R}\right)^B \exp\left(\frac{-E_a'}{T}\right) \tag{B.4}$$

$$k_{\mathrm{inf}} = A' \left(\frac{T}{T_R'}\right)^B \exp\left(\frac{-E_a}{T}\right) \tag{B.5}$$

$$G = \left[1 + \left(\frac{\log(k_0[M]/k_{\mathrm{inf}})}{n}\right)^2\right]^{-1} \tag{B.6}$$

$$k_{eff} = f \left[\frac{k_0[M]}{1 + k_0[M]/k_{\mathrm{inf}}}\right] F^G \tag{B.7}$$

$$\tag{B.8}$$

with T_R a reference temperature (K), E_a an Arrhenius activation energy (K), $[M]$ the concentration of air (molec/cm3), k_0 the low pressure limit of the reaction rate, k_{inf} the high pressure limit of the reaction rate, f is a conversion factor from molec/cm^3 to ppb/min and $\log$ is the 10-based logarithm.

Table B.3 shows reaction rates for all non-photolytic reactions in the CBM-IV scheme. Reaction rates (ppb^{-x} min^{-1}) are coded as follows:

- AE: $R_k = A \exp[-E/(RT)]$

- Parameters $k_0 + k_{inf} + F + n + f$ are parameters for Troe formulas, with $E_a = 0K, T_R = 300K$; k_0, k_{inf} coded as AB̂.

- x is the order of the reaction and T the temperature in Kelvin.

H2O is the water concentration in ppm.Note the use of conversion factors for conversion of 1 ppb = 2.7×10^{10} or 2.46^{10} molec/cm^3, 1 minute = 60 seconds and 1 ppm = 1000 ppb for [H2O]

Table B.3   Reactions and rates for non-photolytic reactions in the CBM-IV mechanism, as used in LOTOS-EUROS.

Label	Reactants	Products	Rate Expression
R3	O3+NO	NO2	2.64 @ 1450
R7	NO2+O3	NO3	0.176 @ 2450
R10	O3+OH	HO2	2.362 @ 940
R11	O3+HO2	OH	2.1E-2 @ 580
R12	NO3+NO	2*NO2	19.09 @ -250
R13	NO3+NO2	NO + NO2	3.66E-2 @ 1230
R14	NO3+NO2	N2O5	0.785 @ -256
R15 [a]	N2O5 + H2O	2*HNO3	1.92E-6
R17	NO+NO2+H2O	2*HNO2	1.68E-20 @-6348
R18	HNO2+HNO2	NO + NO2	1.48E-8
R20	NO2+OH	HNO3	1.537 @ -713
R21	NO+OH	HNO2	6.554E-1 @ -806
R22	HO2+NO	OH + NO2	5.46 @ -240
R23	NO+NO	2*NO2	2.66E-8 @ -530
R26	OH+HNO2	NO2	9.77
R29	HO2+HO2	H2O2	0.087 @ -1150
R30	HO2+HO2+H2O	H2O2	7.7E-13 @ -5800
R31	OH+CO	HO2	0.322
R32	FORM+OH	HO2 + CO	23.60 @ 110
R36	FORM+NO3	HNO3 + HO2 + CO	9.3E-4
R38	ALD+OH	C2O3	10.33 @ -250
R39	ALD+NO3	C2O3 + HNO3	2.05 @ 1900
R42	C2O3+NO	NO2 + XO2 + FORM + HO2	7.97 @ -250
R43	C2O3+NO2	PAN	9.7E-29⌃5.6 + 9.3E-12Î.5 + 0.6 +1 +60.*2.46E10
R44	PAN	C2O3 + NO2	Rk(43)/(2.46e10*9.0e-29*exp(14000/ T))
R45	C2O3+C2O3	2*FORM + 2*XO2 + 2*HO2	3.7
R46	C2O3+HO2	0.79 * FORM + 0.79 * HO2 + 0.79 * XO2 + 0.79 *OH	0.635 @ -1040

Continued on next page

Table B.3 –continued from previous page

Label	Reactants	Products	Rate Expression
R48	OH+MGLY	XO2 + C2O3	25.1
R49	CH4+OH	XO2 + FORM + HO2	3.91 @ 1800
R50	PAR+OH	ftmp_xo2*XO2 + 0.067*XO2N + ftmp_ho2 *HO2 + ftmp_ald*ALD - ftmp_no2*NO2 - ftmp_par*PAR	1.203
R52	OH+OLE	FORM + ALD + XO2 + HO2 - PAR	7.67 @ -504
R53	O3+OLE	0.500*ALD + 0.660*FORM + 0.212*CO + 0.280*HO2 + 0.080*OH + 0.144*XO2 - PAR	2.066E-2 @ 2105
R54	NO3+OLE	0.910*HO2 + 0.910*XO2 + 0.090*XO2N - PAR	1.137E-2
R56	OH+ETH	XO2 + 2*FORM + HO2	2.95 @ -411
R57	O3+ETH	FORM + 0.370*CO + 0.130*HO2	1.92E-2 @ 2633
R58	TOL+OH	1.130*CO + 1.130*FORM + 0.560*MGLY + 0.360*PAR + 0.360*CRES + HO2 + 0.640*XO2 + 0.560*TO2	3.106 @ -322
R59 [b]	CRES+NO3	CRO + HNO3	32.47
R60	CRO+NO2		20.0
R61	OH+XYL	0.700*HO2 + 1.100*PAR + 0.800*MGLY + 0.200*CRES + 0.300*TO2 + 0.100*XO2	24.53 @ -116
R62	OH+CRES	0.400*CRO + 0.600*XO2N + 0.600*HO2	60.5
R63	XO2+NO	NO2	12.0
R64	XO2N+NO		1.2
R65	XO2+XO2		2.5E-2 @ -1300
R66	XO2+HO2		0.113 @ -1300
R67	XO2N+HO2		0.113 @ -1300
R68	XO2N+XO2N		2.5E-2 @ -1300

Continued on next page

Table B.3 –continued from previous page

Label	Reactants	Products	Rate Expression
R69	XO2+XO2N		5.E-2 @ -1300
R71	SO2+OH	SO4a + HO2	1.5
R72[c]	SO2	SO4a	8.3e-5 $(1 + 2\epsilon)$, for RH ¡ 90
			8.3e-5 $(1 + 2\epsilon)$ $(1+ \frac{RH-90}{1})$, for RH ¿ 90
R73	OH+H2O2	HO2	4.72 @ 187
R76	OH+HNO3	NO3	7.58E-3 @ -1000
R80	OH+ISO	0.91*ISPD + 0.629*FORM + 0.991*XO2 + 0.912*HO2 + 0.088*XO2N	4.06E1 @ -407.6
R81	O3+ISO	0.65*ISPD + 0.600*FORM + 0.066*HO2 + 0.266*OH + 0.200*C2O3 + 0.150*ALD + 0.350*PAR + 0.066*CO	1.26E-2 @ 1912
R82	NO3+ISO	0.2*ISPD + XO2 + 0.800*HO2 + NO2 + 0.800*ALD + 2.400*PAR	4.85 @ 448
R95	TO2+NO	NO2 + 0.900*HO2 + 0.900*OPEN	12.0
R96	TO2	CRES + HO2	2.5E2
R97	OPEN+OH	XO2 + C2O3 + 2*HO2 + 2*CO + FORM	44.0
R98	OPEN+O3	0.030*ALD + 0.620*C2O3 + 0.700*FORM + 0.030*XO2 + 0.690*CO + 0.080*OH + 0.760*HO2 + 0.200*MGLY	8.03E-5 @ 500
R100	NO2+ISO	ISPD + XO2 + 0.800*HO2 + 0.200*NO + 0.800*ALD + 2.400*PAR	2.2E-7
R101	OH+ISPD	1.565*PAR + 0.167*FORM + 0.713*XO2 + 0.500*HO2 + 0.334*CO + 0.168*MGLY + 0.498*C2O3 + 0.273*ALD	49.66
R102	O3+ISPD	0.114*C2O3 + 0.150*FORM + 0.850*MGLY + 0.154*HO2 + 0.266*OH + 0.064*XO2 + 0.360*PAR + 0.225*CO + 0.020*ALD	1.05E-5

Continued on next page

Table B.3 –continued from previous page

Label	Reactants	Products	Rate Expression
R103	NO3+ISPD	0.357*ALD + 0.282*FORM + 1.282*PAR + 0.925*HO2 + 0.643*CO + 0.075*C2O3 + 0.074*XO2 + 0.075*HNO3	1.478E-3

[a] In reaction 15, the water concentration is the water around the aerosol SO4a. In case aerosols are computed, this reaction rate is set to zero, because this reaction is explicitly accounted for in the hegerogeneous chemistry

[b] Reaction 50 lumps reactions 52-55 in Gery et al. (1989). Coefficients ftmp$_-$ depend on temperature and NO_2 concentration.

[c] $\epsilon =$ cloud cover fraction (0-1), RH=relative humidity

C   Secondary organic aerosol with VBS approach

This chapter describes the partitioning formulation, yields for SOA precursors (high-NOx and low-NOx) and description of aging.

C.1   Formation of SOA from VOC

VOCs are highly reactive, and apart from their role in the CBM4 reactions involved in for instance ozone formation, in the VBS extension they also contribute to the formation of secondary organic aerosol (SOA). It is assumed that the aerosol formation is additional and independent to the effect on ozone chemistry. This means that performing a run with VBS turned on or off should give exactly the same result for all the gases. VOCs that are considered to produce SOA are on the one hand the biogenic precursors isoprene (ISO) and monoterpenes (TERP), and on the other hand the anthropogenic precursors xylene (XYL), toluene (TOL), alkanes (PAR), and alkenes (OLE and PAR). The reaction of these precursors, which are emitted in the gas-phase, with radicals (mainly OH) are assumed to produce semi-volatile organic species with saturation concentration (C*) values in the range 10^1-10^4 (i.e. only four out of the nine vbs bins). However, after oxidation the anthopogenic and biogenic SVOC can move to the 2 lowest saturation concentrations bins as well. The total number of species in the VBS related to aVOC and bVOC is 24: 6 species in the gas-phase and in the aerosol phase, respectively, for each category. The SOA species that are formed in the model from anthopogenic and biogenic VOCs are called aSOA and bSOA, respectively.

The SOA yields for the various precursors are taken from Tsimpidi et al. (2010), which is based on fits of smog-chamber experimental results. The relation between our SOA precursors and those from Tsimpidi et al. (2010) is shown in TableC.3. Note that four of the precursors are equivalent, and the only difference is in the PAR and OLE precursors, which is due to the difference between our carbon-based chemistry and the SAPRC99 chemistry used by Tsimpidi et al. (2010). For example, using a molecular weight of on average 135 g/mol for Tsimpidi's ALK4 and ALK5 compounds (their Table 2), the PAR molecular weight is about 9-fold lower (which we rounded to 10). Although the factor of 10 is probably incorrect (some of the PARs should also go into alkenes), the yields of alkanes and alkenes are anyway low so they don't have a large role for the SOA production. Hence, so far we did not attempt to make a more educated guess. The yields from the various precursors given in Table 3 are mass-based,e.g., 1 $\mu g/m^3$ of isoprene gives rise to 0.023 $\mu g/m^3$ of material in the vbs class with C*=10 $\mu g/m^3$.

Table C.1   VBS aerosol phasse species in LOTOS-EUROS

C_i*	10^{-2}	10^{-1}	1	10	10^2	10^3	10^4	10^5	10^6
aVOC	aSOA1	aSOA2	aSOA3	aSOA4	aSOA5	aSOA6	-	-	-
bVOC	bSOA1	bSOA2	bSOA3	bSOA4	bSOA5	bSOA6	-	-	-
POA	POA1	POA2	POA3	POA4	POA5	POA6	POA7	POA8	POA9
SOA	siSOA1	siSOA2	siSOA3	siSOA4	siSOA5	siSOA6	siSOA7	siSOA8	-

Table C.2   Volatility classes and the mass fraction of POM entering these classes

C_i*	10^{-2}	10^{-1}	1	10	10^2	$10^3$3	10^4	10^5	10^6
fraction of POA emission	0.1	0.2	0.3	0.4	0.1	0.2	0.3	0.4	0.5

Table C.3   Relation between SOA yields for LE precursors and those for the Tsimpidi precursors

Lotos-Euros	TERP	ISO	ARO1	ARO2	PAR	OLE
Tsimpidi	TERP	ISOP	TOL	XYL	0.5*(ALK4+ALK5)/10	0.5*(OLE1+OLE2)/10

Table C.4   Mass-based yields for SOA precursors,after translation from Tsimpidi et al. (2010) to LOTOS-EUROS

SOA precursor	High-NOx parameterization				Low-Nox parameterization			
	1	10	100	1000	1	10	100	1000
PAR	0.000	0.094/10	0.000	0.000	0.000	0.1875/10	0.000	0.000
OLE	0.002/10	0.0155/10	0.0605/10	0.210/10	0.014/10	0.0865/10	0.0945/10	0.300/10
TOL	0.003	0.165	0.300	0.435	0.075	0.225	0.375	0.525
XYL	0.002	0.195	0.300	0.435	0.075	0.300	0.375	0.525
ISO	0.001	0.023	0.015	0.0	0.009	0.030	0.015	0.000
TERP	0.012	0.122	0.201	0.500	0.092	0.092	0.359	0.600

The SOA yields are split into a low-NOx and a high-NOx case as first suggested by Lane et al. (2008).The mass-based yield y of a VOC is defined as a linear combination of its high-NOx (y_{high}) and low-NOx (y_{low}) yield: $y = y_{high}B + y_{low}(1 - B)$, where B is the 'branching ratio, i.e. a measure of which fraction of the reactions takes place with the NO radical. Typically, the calculation of the branching ratio is performed as in Lane et al. (2008) and in Farina and Adams (2010):

$$B = \frac{k_{RO_2+NO}[RO_2][NO]}{k_{RO_2+NO}[RO_2][NO] + k_{RO_2+RO_2}[RO_2][RO_2] + k_{RO_2+RO_2}[RO_2][HO_2])} \quad \text{(C.1)}$$

where the k parameters are rates for the various reactions considered. However, in LOTOS-EUROS we do not explicitly describe a precursor radical for each precursor, and this would have quite an impact on the chemistry scheme. Considering that the step from the precursors to the intermediate RO2 radicals is very fast, and that the amount of precursor giving rise to VBS product then approximates the RO2 concentration. Thus, the [RO2] in the above equation is replaced by the amount of precursor gas that reacted (termed ΔROG, see below). Moreover, the CMB-IV (see also Appendix B reactions with the XO2 species (which is used for NO to NO2 conversion from an RO2 radical) are used as reaction rates within the branching ratio equation for each precursor. These reactions are: XO2+NO→NO2 (reaction 63), XO2+XO2→. . . (reaction 65), and XO2+HO2→. . . (reaction 66). Additionally, we simplify by assuming that the RO2 self-reaction is very slow and therefore negliglible the above equation.

Note that turning on VBS calculations will strongly affect terpene concentrations because the loss reactions of terpene with radicals will now be included. Therefore, we decided to conserve the oxidant concentrations in the terpene reaction by including them as a reaction product.

The output from SOA chemistry that is required for further vbs calculations, is the amount of precursor gas that reacted, because a fraction of this mass subsequently gives rise to vbs products. The amount of reacted precursor is also termed ΔROG (change in Reactive Oxygen Gas). For the precursors TERP, ISO, TOL, XYL, and OLE this is easily determined by calculating the difference in concentration just after and just before the chemistry step. Note that this can be done because these precursors are only consumed in the reaction scheme, and are not formed. For the PAR precursor this is different because in several reactions it is formed as well. Thus, the for PAR the Δ ROG is approximated within the TWOSTEP routine by multiplying for all loss reactions the reaction rates with the concentrations of the involved reactants. These include the reactions of PAR with OH (reaction 50), OLE with OH (reaction 52), OLE with O3 (reaction 53), and OLE with NO3 (reaction 54). The latter three reactions are special because PAR is assumed to be produced at a negative rate so this actually means a loss of PAR (these represent composite reactions where only in a very fast intermediate step PAR is lost such that the PAR concentration should not affect the reaction rate). The calculated ΔROGs are input for the yield calculations. The NOx dependence of the yields as described above are also calculated in that file. The mass-based yields from literature are recalculated into ppb yields using the molecular weights of the precursors and of the vbs products.

C.2   Formation of POA and SOA from primary emissions

In addition to SOA formation from VOCs, we include emissions of organic matter (OM) from anthropogenic sources, as well as formation of SOA from the semi- and intermediate volatile compounds that result from evaporation of these primary emissions. The part of OM that stays in the aerosol phase is called primary organic aerosol (POA) in the VBS. The part of OC that evaporates upon emission and dilution in the atmosphere forms semi-volatile and intermediate volatile organic species (SVOC and IVOC, respectively). SVOC and IVOC are defined by their volatility: SVOC have $10^0 < C* < 10^2 \mu g/m^3$ at 298K and IVOC have $10^3 < C^* < 10^6 \mu g/m^3$ at 298K. When SVOC and IVOC (together called S/IVOC) are oxidized in the atmosphere, their volatility decreases and they will partition between the gas and the aerosol phase, forming SOA. In the model, we call this siSOA. In the VBS, we keep track of primary and secondary products that result from the OC emissions separately, both in the gas and in the aerosol phase (34) species in total). The emissions of OM are divided over the 9 volatility classes as follows: the 4 lowest bins receive in total 1x the OM emissions, and the 5 other bins receive in total 1.5x the OM emissions, with the latter representing a best guess estimate for the IVOC emissions that are usually not included in POM inventories (see TableC.2).

C.3   Partitioning

Distributing the material in a class between the gas and the aerosol phase (partitioning) occurs following Donahue et al. (2006). Thus, the fraction of mass in aerosol phase ξ_i is calculated using:

$$\xi_i = \frac{1}{1 + \frac{C_i^*}{C_{OA}}} \tag{C.2}$$

where C_i is the mass concentration ($\mu g/m^3$) in VBS class i with saturation concentrations C_i^* ($\mu g/m^3$) for the current temperature (see below), and $C_{OA} = \sum_i C_i \xi_i$ (i.e., C_{OA} is the total mass concentration of material in aerosol phase in all VBS classes). Because the fraction of material in aerosol phase within a class depends on the total mass concentration in aerosol phase, these two variables are dependent and can only be determined iteratively.

At the reference temperature (currently set at 313 K, usually 300 K or 298 K is used), the saturation vapor pressures (C* values) of the VBS classes are defined logarithmically. These saturation vapor pressures depend on temperature according to the Clausius-Clapeyron equation:

$$C_i^*(T) = C_i^*(T_0)(T_0/T)e^{\Delta H_{vap/R}(1/T_0 - 1/T)} \tag{C.3}$$

where T_0 is the reference temperature (K), T is the ambient temperature (K), R is the universal gas constant (J/mol/K) and ΔH_{vap} is the effective heat of vaporization (J/mol). Various authors have tried distinct values for ΔH_{vap}, and a typical choice is 30 kJ/mol. Because we take ΔH_{vap} equal for all volatility classes, within one grid cell the C* values of the classes remain logarithmically spaced independent of temperature. Some authors use distinct values for ΔH_{vap} between the vbs classes (e.g., Tsimpidi et al. (2010)).

C.4　　Aging reactions with OH

The SVOC and IVOC in the VBS bins react with the OH radical giving rise to increasingly oxygenated species. It is assumed that the gas phase species become less volatile due to this 'aging', and therefore material is shifted towards lower-volatility VBS bins. In general the reactions can be described as $CG_x + OH \rightarrow CG_{x-1}$ occurring at rate k (we use values of $4*10^{-11}$, $1*10^{-11}$ and 0 cm^3/molecule/s for S/IVOC, aVOC and bVOC, respectively). These aging reactions are included in the chemical scheme. To account for added oxygen, a small mass increase of 7.5% during aging reactions is included (e.g., Tsimpidi et al. (2010)). Note that this means that there is no mass conservation during aging. We assume that no aging occurs in the particle phase.

C.5　　Deposition of vbs species

Wet and dry deposition of aerosol is done analogous to conventional aerosols: aerosol phase species are treated as coarse mode aerosol. Dry and wet deposition of condensable gases are taken into account using surface resistance, uptake by vegetation and wash-out ratios). To account for mesophyll conductance, which is a potentially important deposition path for soluble organic species, we applied the dependencies on solubility and reactivity from Wesely (1989). Note that we applied this deposition pathways for S/IVOC species only, since it has not been applied to all CBM4 species when using the model without VBS.